FOCUSING ON ACOUSTIC WAVES IN A NON-UNIFORM ATMOSPHERE

G.E. SMITH

MATERIALS RESEARCH LABORATORY
DSTO

FOCUSING OF ACOUSTIC WAVES IN A NON-UNIFORM ATMOSPHERE

G.E. Smith

MRL Technical Report
MRL-TR-89-10

ABSTRACT

The blast scaling principle by charge weights may often produce gross errors in the estimation of overpressures at significant distances from a shot site. The principle ignores weather conditions and assumes a homogeneous atmosphere. Weather conditions may cause variations in the velocity of sound which allows the atmosphere to refract sound waves and act as an acoustic lens. Certain weather conditions such as temperature inversions may allow an acoustic focus many kilometres away from a shot site. Acoustic propagation from a noise producing installation has been mathematically modelled to assist in the prediction of anomalous overpressures by acoustic focusing. ~~MRL has developed~~ a computer model, REFFOCUS, to illustrate foci in a vertically inhomogeneous, non-turbulent, moving atmosphere. The model is produced from sound velocity profiles derived primarily from temperature and wind shear profiles.

was developed

Published by Materials Research Laboratory
Cordite Avenue, Maribyrnong, Victoria 3032, Australia
Telephone: (03) 319 3887
Fax: (03) 318 4536

AR No. 005-695

Approved for public release

AUTHOR

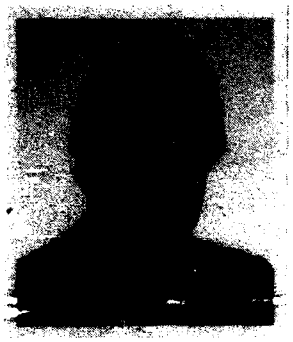

Gil Smith graduated in Physics from the University of NSW in 1982. He joined Telectronics Pty Ltd in 1983 in pacemaker and prosthesis research. After completing a Graduate Dip Ed at Newcastle CAE in 1984, he studied metal hydrides at Newcastle University while teaching in schools and TAFE. He enrolled in a Masters Qualification (Physics Hons) at Newcastle University which was completed in 1986. After lecturing for two years in physics and radiography at Newcastle CAE he joined MRL in 1988 to study blast propagation in the atmosphere, fragment impact on explosives, and optical fibre instrumentation.

CONTENTS

FOCUSING OF ACOUSTIC WAVES IN A NON-UNIFORM ATMOSPHERE

1. INTRODUCTION

Anomalous overpressures, larger or smaller than expected, may be manifest adjacent to, or at relatively large distances from, the boundaries of an explosives or noise producing installation. Although of relatively low intensity, these focused shock waves may be avoided by ensuring favourable weather conditions. The purpose of this report is to produce a model to predict acoustic focused events as a function of the acoustic properties of the atmosphere.

Normally, assuming a surface burst (or surface noise generator) and depending upon the amount of absorption and cratering of the surface, from 50 to 100% of the energy generated by an explosion may be transmitted radially from the shot site. There are numerous conflicting theoretical and empirical equations which have been employed to calculate the energy and overpressures at any given radius from the shot site (Baker, 1973). However, these calculations are known to underestimate observed values at focused events and to overestimate observed values in the quiet zones in between. The assumption of the continuous divergence of blast energy at extended range is in error with the detection of energy concentrations at foci. Remote from the shot site, overpressures are relatively low and may be regarded as perturbations in the ambient pressure so that the speed of a front is approximately acoustic (Cox et al., 1952) and the front will obey the laws of acoustics. Derivations and calculations in this report assume acoustic propagation away from the shot site and are concerned with the prevailing weather conditions producing an acoustic lens within the layers of the atmosphere.

2. FACTORS AFFECTING ACOUSTIC FOCUSING

2.1 Velocity of Sound - Temperature, Wind, Humidity Effects

2.1.1 Temperature Effects

The equation for the speed of sound, v, in a homogeneous still atmosphere can be reduced to (Herman et al., 1983):

$$v = (1 + 0.26\ q)\ (RT\gamma)^{1/2} \qquad \text{(m/s)} \qquad (1)$$

where $\gamma = C_p/C_v$ = ratio of specific heats at constant pressure and temperature in dry air;
R = specific gas constant in dry air = 287.05 (J kg^{-1} K^{-1});
T = temperature (K);
q = specific humidity (kg/kg of moist air).

Figure 1 shows a variation in the velocity of sound due to atmospheric temperature gradients. An increase in temperature will result in an increased sonic velocity.

2.1.2 Humidity Effects

The contribution to sonic velocity from humidity is below 1% at normal temperatures and may be neglected (Herman et al).

2.1.3 Wind Shear Effects

Wind velocities may have a significant effect on the velocity of sound as predicted by the above equation. In a static atmosphere a sound wave will be allowed to travel through each medium with a wave velocity as prescribed by the prevailing temperature and humidity effects. However, in a non-turbulent, moving atmosphere each medium has a velocity with respect to the ground so that sound wave velocity components and the corresponding wind velocity components may be summed vectorially (Fig. 1). This means high winds may markedly alter acoustic velocities from very low to quite large sound velocities. Therefore, along with temperature profile effects, wind shear effects are a major contributor to the question of noise focusing in the atmosphere. The component of the wind velocity which is of interest is the one that moves along the path taken by the propagating sound front.

2.2 Energy Tubes and Overpressure

It is convenient to indicate the direction of the energy flow by a series of acoustic ray paths of equal angular displacement which radiate out from the shot site and remain at all times normal to the blast front. In this fashion an inhomogeneous atmosphere may be indicated by ray paths which deviate from straight radial paths diverging from the shot site (Figs 2-4). Because these rays are traced along the flow of energy, then energy radiating from the shot site within some solid angle remains within their bounds - this region may be called an energy tube (Sach, 1961). Although it is not anticipated that the energy within a tube will flow normal to the bounding rays of the tube wall, it is possible that two or more energy tubes may intersect to produce a focus. However, there is atmospheric attenuation within each energy tube due to viscosity, the exchange of translational and rotational energy between colliding molecules, and thermal heating and conduction effects particularly near the shot site where pressure gradients and wave velocites are the greatest.

Since overpressure is related to the energy per unit area, then the overpressure at a given range may be calculated. If the energy passes through a large area then the overpressure is reduced. Conversely, if the energy passes into a smaller area then the overpressure is increased to the extent that a point may be provided with energy from a number of tubes at varying angles to produce a focus.

2.3 Acoustic Reflection

The acoustic impedance, Z, of a material is a product of the velocity of sound, v, in the material and its density, ρ.

$$Z = \rho v. \tag{2}$$

The fraction of energy reflected at a normal to the boundary between two media of acoustic impedances Z_1 and Z_2 is:

$$E_R = \frac{(Z_2 - Z_1)^2}{(Z_1 + Z_2)^2} . \tag{3}$$

The fraction of energy refracted (transmitted) through the boundary is:

$$E_T = \frac{4Z_1Z_2}{(Z_1 + Z_2)^2} . \tag{4}$$

At the boundary between adjacent heights within one atmospheric layer possessing a linear velocity profile, or at the boundary between two layers with similar sound velocities and acoustic impedances ($Z_1 \approx Z_2$), reflection of the sound front normal to the boundary will be a minimum - e.g. cloud and meteorological discontinuities - and $E_R \approx 0$, $E_T \approx 1$.

There is a maximum of reflection of the sound front at the boundary between media of greatly different acoustic impedance ($Z_1 \gg Z_2$ or $Z_1 \ll Z_2$) - e.g. air and ground - and $E_R \approx 1$, $E_T \approx 0$. Note, the reflected plus refracted energy is ideally equal to the incident energy so that:

$$E_R + E_T = 1 \tag{5}$$

depending upon attenuation effects.

2.4 Acoustic Diffraction

Diffraction of a sound wave would require very large overpressures found in shock fronts near the shot site to become significant in the attenuation of sound wave energy. However, at extended ranges the overpressures are relatively small and front velocities are approximately the speed of sound (Whitham, 1957). In the present study we therefore neglect the effects of diffraction.

2.5 Acoustic Refraction

Refraction through the atmosphere contributes to the focusing of blast energies at extended ranges. Section 3 details the equations governing the path of sound rays orthogonal to the surface of an acoustic front through a vertically inhomogeneous, stratified, moving atmosphere.

For each azimuth and within each atmospheric layer there can be defined a sound velocity profile, $K = dv/dy$, which is the change in sound velocity with altitude. Within the ith atmospheric layer bounded by a higher altitude sound velocity, v_{i+1}, and a lower altitude sound velocity v_i, there will be a sound velocity profile K_i where all refracted sound rays behave as follows:

K	Condition	Refraction	Figure No.
$K_i < 0$	$v_{i+1} < v_i$	Upward	Figure 2
$K_i = 0$	$v_{i+1} = v_i$	Not refracted	Figure 3
$K_i > 0$	$v_{i+1} > v_i$	Downward	Figure 4

Generally a ray will be turned toward regions where the sound velocity is lower. According to a Huygens-Kirchhoff construction, every point on a moving wave front of arbitrary shape at an instant t is the source of secondary, outward-propagating spherical wavelets of variable phase and of radius $v\delta t$. Where v is larger, $v\delta t$ and the radius of the wavelet is larger. The tangents of the forward-going portions of these wavelets of different radii produce an envelope which defines the advancing wave front at time $t + \delta t$. The wave front, having already advanced further in the region of higher velocity, will bend toward the region of lower velocity.

Ground focusing requires the presence of stratified atmospheric layers with sound velocity profiles such that:

(i) some sound velocity is greater at a higher altitude than at the ground - this is the primary condition for a focused event;

(ii) a collection of rays at various angles are incident at the same range, and arrive at the same time and in-phase (according to Fermat's principle of least time) so that they superimpose to produce a large overpressure.

3. RAY MECHANICS OF ATMOSPHERIC REFRACTION

The ray of an acoustic front has slope, y':

$$y' = \frac{dy}{dx} = \tan\theta \qquad (6)$$

where θ = angular displacement from the horizontal;
y = vertical displacement from the shot site;

x = horixontal displacement from the shot site.

The rate of change in slope, y', of the blast front ray is:

$$y'' = \frac{dy'}{dx} = \frac{d(\tan\theta)}{dx} \tag{7}$$

Snell's law for two different media (e.g. two air layers) describes the relationship between velocity and direction components (Fig. 5a)

$$\frac{\sin(90^{o} - \theta_i)}{v_i} = \frac{\sin(90^{o} - \theta_{i+1})}{v_{i+1}} = c = \text{constant}$$

where i = 1, 2, 3, ..., n;

n is the number of atmospheric layers;

v_i is the initial sound velocity in the ith layer;

v_{i+1} is the initial sound velocity in the (i + 1)th layer and is equal to the final sound velocity in the ith layer;

θ_i is the initial angular displacement from the horizontal in the ith layer;

θ_{i+1} is the initial angular displacement from the horizontal in the (i + 1)th layer.

Thus

$$\frac{\cos\theta_i}{v_i} = \frac{\cos\theta_{i+1}}{v_{i+1}} = c \tag{8}$$

Snell's law may be iterated through each layer to the shot site so that:

$$\frac{v_1}{\cos\theta_1} = \frac{v_i}{\cos\theta_i} \tag{9}$$

where: v_1 is the initial sound velocity in the first layer (at the shot site);

θ_1 is the initial angular displacement from the horizontal in the first layer.

It should be noted that Eqn. (9) holds equally well within individual layers if the subscripts are allowed to identify sound velocities and angles at a given height. Because of the relatively large acoustic propagations involved Eqn. (9) assumes that a blast wave is acoustic in behaviour at the origin. Generally, from figure 5b and Eqn (8)

$$\cos\theta_i = v_i c \tag{10}$$

and,

$$\sin\theta_i = (1 - (v_i c)^2)^{1/2} \tag{11}$$

If there exists a ray which turns over just within the upper boundary of (i - 1)th layer, then $\theta_i = 0$, and $\cos\theta_i = 1$.

So there is a critical angle, θ_{1crit}, coinciding with the maximum angle in layer 1 which will produce a grazing ray at the top of the (i - 1)th layer (bottom of the ith layer), so that:

$$v_i = \frac{v_1}{\cos\theta_{1crit}} \tag{12a}$$

Further, any ray which turns over in any layer so that it returns to the ground has a velocity, v_i, at the top of the arc and must leave the shot site at an angle less than or equal to θ_{1crit}. Otherwise the ray will not turn over and Cos $\theta_i = 1$, i.e. there is some sound velocity greater than v_i at a lower altitude.

So:

$$v_i = \frac{v_1}{\cos\theta_1} \tag{12b}$$

where $\theta_1 \leq \theta_{1crit}$ for the layer. Otherwise Eqn. (9) applies.

3.1 Ray Trace

For the ith layer, substitute Eqns. (10) and (11) into Eqn. (6),

$$y' = \tan\theta = \frac{\sin\theta}{\cos\theta}$$

$$= \frac{(1 - (vc)^2)^{1/2}}{vc} \qquad \text{(see Figure 5b)}$$

$$= (1/(vc)^2 - 1)^{1/2}. \tag{13}$$

Also for the ith layer, substitute Eqn. (7), using partial derivatives:

$$y'' = \frac{dy'}{dx} = \frac{dy'}{d\theta}\,\frac{d\theta}{dv}\,\frac{dy}{dx}\,\frac{dv}{dy}$$

Since $\cos\theta = vc$ from Eqn. (10),

$$-\sin\theta d\theta = c dv$$

and hence

$$\frac{d\theta}{dv} = -\frac{c}{\sin\theta} .$$

Also from Eqn. (6),

$$\frac{dy'}{d\theta} = \sec^2\theta$$

$$y'' = \sec^2\theta \times \frac{-c}{\sin\theta} \frac{\sin\theta}{cv} \frac{dv}{dy}$$

$$= -\frac{\sec^2\theta}{v} \frac{dv}{dy}$$

$$= -\frac{(1 + \tan^2\theta)}{v} \frac{dv}{dy}$$

so

$$y'' = -\frac{(1 + (y')^2)}{v} \frac{dv}{dy} \qquad (14)$$

If the variation of the velocity of sound with height, dv/dy, is assumed to be constant in each atmospheric layer, i.e.

$$\frac{dv}{dy} = K_i = \text{constant}$$

then

$$v_{i+1} - v_i = K_i (h_{i+1} - h_i)$$

and

$$v_{i+1} = K_i y + v_i . \qquad (15)$$

Here the height, y, traversed in the ith atmospheric layer is:

$$y = h_{i+1} - h_i \qquad (16)$$

where h_i is the initial height at the origin of the ray in the ith level;

h_{i+1} is the final height of the ray in the ith level.

By Eqn. (15) the velocity, v, throughout the layer is:

$$v = v_i + K_i\, y$$

and

$$y'' = -\frac{(1 + (y')^2)K_i}{(K_i(y + v_i/K_i))}$$

$$= -\frac{(1 + (y')^2)}{y + v_i/K_i}, \qquad \text{for} \quad K_i \neq 0. \tag{17}$$

The case $K_i = 0$ will be addressed later.

Equation (17) is a nonlinear, inhomogeneous differential equation. A solution is:

$$(x - x_i)^2 + (y + v_i/K_i)^2 = r_i^2 \tag{18}$$

which is illustrated in figure 6a. This is a circle, centre = $(x_i, -v_i/K_i)$, radius = r_i, where x_i and r_i are constants of integration. x_i is the x cartesian coordinate where a ray is at a maximum for $K_i > 0$, or at a minimum for $K_i < 0$ (i.e. slope = 0), and r_i is the radius of curvature of the ray.

It should be noted that the centre of the circle describing the ray's path is vertically displaced by $-v_i/K_i$ from the height of the origin of the ray in the ith layer, and horizontally displaced by x_i. If K_i is positive, then $x_i = v_i \tan\theta_i/K_i$ is + ve, and $-v_i/K_i$ is - ve; if K_i is negative, then x_i is - ve and v_i/K_i is + ve. In cartesian coordinates, with the origin being the point at which the ray enters the atmospheric layer (or the shot site), a ray path with a positive K is a circle with a centre to the right and below the origin (4th quadrant) - the ray is refracted toward the ground as shown in figure 6a. A ray path with a negative K is a circle with a centre to the left and above the origin (2nd quadrant) - the ray is refracted upward as shown in figure 6b.

It should be noted that there are theoretical points in both figures 6a and 6b where the sound ray has an infinite slope and the velocity of sound is zero. This follows from Eqn. (9) where the second angle is $\theta_2 = 90^\circ$ ($\cos\theta_2 = 0$). Also there are points where the sound ray turns over with a slope of zero and the velocity of sound is a maximum - by Eqn. (9) when $\theta_2 = 0$ ($\cos\theta_2 = 1$).

We now present examples of the application of the solution to one, two, three and n atmospheric layers where the $K_i \neq 0$.

3.1.1 1 Atmospheric Layer

From Eqn. (18) (Figure 6a and 6b)

$$(x - x_1)^2 + (y - h_1 + v_1/K_1)^2 = r_1^2 \tag{19}$$

where h_1 is the height of the origin of the ray in the first layer (the shot site). Boundary conditions at the maximum (+ ve K) or the minimum (- ve K) are:

$$x = x_1,\ y - h_1 = y_1,\ \text{so } r_1^2 = (y_1 + v_1/K_1)^2$$

$$= (v_2/K_1)^2.$$

The ray turns over if it is allowed to travel only in this layer from Eqns. (12b) and (15):

$$(x - x_1)^2 + (y - h_1 + v_1/K_1)^2 = + \frac{v_1^2}{(K_1 \cos\ \theta_1)^2}\ . \tag{20}$$

Equation (12b) is true for any ray which turns over in the ith layer with an angle less than the critical angle (any instantaneous ray angle or sound velocity in the ith layer can be described by Eqn. (8)). Rearranging the circle, Eqn. (20) gives

$$y = h_1 - \frac{v_1}{K_1} \pm \sqrt{\frac{v_1^2}{(K_1 \cos\theta_1)^2} - (x - x_1)^2} \tag{21}$$

where the square root is to be given the same sign as K.

3.1.2 2 Atmospheric Layers

Refer to figure 5a substituting 1=i, 2=i+1 with positive sound velocity profile and figure 7 with negative sound velocity profiles.

The equation of the first circle for arc AB is now

$$(x - x_1)^2 + (y - h_1 + v_1/K_1)^2 = \frac{v_1^2}{(K_1 \cos\theta_1)^2}$$

If K_1 is positive then:

$$x \leq X_1 \tag{22}$$

where: x_1 is now the horizontal displacement of the ray in the first layer, before turnover;

X_1 is the horizontal displacement of the centre of the circle from the origin - positive for $K_1 > 0$, negative for $K_1 < 0$.

Equation (21) becomes:

$$y = h_1 - \frac{v_1}{K_1} \pm \sqrt{\frac{v_1^2}{(K_1 \cos\theta_1)^2} - (x - X_1)^2} \quad . \tag{23}$$

The equation of the second circle for arc BC is:

$$(x - \{x_1 + X_2\})^2 + (y - h_2 + v_2/K_2)^2 = \frac{v_1^2}{(K_2 \cos\theta_1)^2} \quad . \tag{24}$$

If K_2 is positive then:

$$x_1 \leq x \leq x_1 + X_2$$

and $X_2 \geq x_2$

where: x_2 is the horizontal displacement of the ray, from the origin of the ray in layer 2, before turnover;

X_2 is the horizontal displacement of the centre of the circle from the origin of the ray in layer 2 - positive for $K_2 > 0$, negative for $K_2 < 0$;

h_2 is the height of the origin of the ray in the second layer.

So:

$$y = h_2 - \frac{v_2}{K_2} \pm \sqrt{\frac{v_1^2}{(K_2 \cos\theta_1)^2} - (x - \{x_1 + X_2\})^2} \quad . \tag{25}$$

3.1.3 3 Atmospheric Layers

Refer to figure 8 with positive sound velocity profiles.

The equation of the circle for arc AB is now:

$$(x - X_1)^2 + (y - h_1 + v_1/K_1)^2 = \frac{v_1^2}{(K_1 \cos\theta_1)^2} \quad .$$

If K_1 is positive then

$$x \leq x_1$$

The equation of the second circle for arc BC is:

$$(x - \{x_1 + X_2\})^2 + (y - h_2 + v_2/K_2)^2 = \frac{v_1^2}{(K_2\cos\theta_1)^2} .$$

If K_2 us positive then:

$$x_1 \leq x \leq x_1 + X_2$$

and $X_2 \geq x_2$

The equation of the third circle for arc CD is:

$$(x - \{x_1 + x_2 + X_3\})^2 + (y - h_3 + v_3/K_3)^2 = \frac{v_1^2}{(K_2\cos\theta_1)^2} \qquad (26)$$

If K_3 is positive then:

$$x_1 + x_2 \leq x \leq x_1 + x_2 + X_3$$

and $X_3 \geq x_3$

where: x_3 is the horizontal displacement of the ray, from the origin of the ray in layer 3, before turnover;

X_3 is the horizontal displacement of the centre of the circle from the origin of the ray in layer 3 - positive for $K_3 > 0$, negative for $K_3 < 0$;

h_3 is the height of the origin of the ray in the third layer.

So:

$$y = h_3 - \frac{v_3}{K_3} \pm \sqrt{\frac{v_1^2}{(K_3\cos\theta_1)^2} - (x - \{x_1 + x_2 - X_3\})^2} \qquad (27)$$

3.1.4 n Atmospheric Layers

Similarly, the equation of the nth circle for the nth arc is:

$$(x - \{[\sum_{i=1}^{n-1} x_i] + X_n\})^2 + (y - h_n + v_n/K_n)^2 = \frac{v_1^2}{(K_2 \cos\theta_1)^2}$$

If K_n is positive then:

$$\sum_{i=1}^{n-1} x_i \leq x \leq [\sum_{i=1}^{n-1} x_i] + X_n$$

and $X_n \geq x_n$ and $K_i \neq 0$ (28)

where: x_n is the horizontal displacement of the ray, from the origin of the ray in the nth layer, before turnover;

X_n is the horizontal displacement of the centre of the circle from the origin of the ray in the nth layer – positive for $K_n > 0$, negative for $K_n < 0$;

h_n is the height of the origin of the ray in the nth layer.

So:

$$y = h_n - \frac{v_n}{K_n} \pm \sqrt{\frac{v_1^2}{(K_n \cos\theta_1)^2} - (x - \{[\sum_{i=1}^{n-1} x_i] + X_n\})^2} \quad (29)$$

If K_n is positive then

$$\sum_{i=1}^{n-1} x_i \leq x \leq [\sum_{i=1}^{n-1} x_i] + X_n$$

and $X_n \geq x_n$ and $K_i \neq 0$.

The square root term is to be given the same sign as K.

Equations (19) through (29) hold for $K_i \neq 0$.

3.1.5 Layers with Zero Velocity Profiles

If $K_i = 0$, then by trigonometry, figure 9

$$x_m = \frac{y_m}{\tan\theta_m} \qquad \text{For } i = m < n \quad (30)$$

Generally for n layers, if $K_i = 0$, and $i = m < n$ the cartesian coordinates are:

$$y = h_m + x_m \tan\theta_m + (h_n - h_{m+1}) \tag{31}$$

and

$$x = \left[\sum_{i=1}^{m-1} x_i\right] + \frac{y_m}{\tan\theta_m} + \left[\sum_{i=m+1}^{n-1} x_i\right] \tag{32}$$

The first terms in Eqns. (31) and (32) are calculated using Eqn. (28) up to the (m - 1)th layer, and the second terms are calculated by trigonometry for the case where $K_m = 0$. The third terms may be calculated using Eqn. (28) for the (m + 1)th to nth layers. The number of terms is dictated by the number of non-adjacent zero velocity profiles.

3.2 Range

If a ray turns over in the ith atmospheric layer, the height traversed by the ray in the layer is given by Eqn. (16):

$$y = h_{i+1} - h_i$$

The velocity along the ray path, v, after height y is:

$$v = v_i + K_i y \tag{33}$$

where: v_i is the initial velocity in the ith layer;
K_i is the velocity gradient in the ith layer.

In any atmospheric layer; Eqn. 10 gives

$$\cos\theta = vc.$$

Now, from Eqn. (6) and trigonometric relations:

$$y' = \tan\theta = \sec^2\theta - 1$$

and

$$\cos\theta = \frac{1}{\sqrt{(\sec^2\theta)}}$$

Then:

$$\cos\theta = \frac{1}{\sqrt{(1 + y'^2)}} \tag{34}$$

By geometry, figure 5b

$$y' = \tan\theta = \pm \frac{cv}{\sqrt{(1 - c^2 v^2)}} \tag{35}$$

and therefore

$$\sum_{i=1}^{n} x_i = \sum_{i=1}^{n} \int_{x_i}^{x_{i+1}} dx = \pm \sum_{i=1}^{n} \int_{y_i}^{y_{i+1}} \frac{cv}{\sqrt{(1 - c^2 v^2)}}\, dy. \tag{36}$$

For the case when $K_i = 0$, substitute:

$$cv = \cos\theta$$
$$cdv = cK_i dy = -\sin\theta d\theta$$

We know that when

$$y = h_i, \qquad \theta = \theta_i$$

and

$$y = h_{i+1}, \qquad \theta = \theta_{i+1}.$$

(Note: The case for $K_i = 0$ will be examined later).

Since the range of a ray which returns to the same height is twice the horizontal displacements through all the atmospheric layers, then:

$$R_n = 2 \sum_{i=1}^{n} x_i. \tag{37}$$

From Eqn. (36)

$$R_n = \pm 2 \sum_{i=1}^{n} \frac{1}{cK_i} \int_{\theta_i}^{\theta_{i+1}} - \frac{\cos\theta \sin\theta d\theta}{\sin\theta}$$

$$= \pm 2 \sum_{i=1}^{n} \frac{1}{cK_i} \int_{\theta_i}^{\theta_{i+1}} - \cos\theta d\theta. \tag{38}$$

Thus

$$R_n = \pm 2 \sum_{i=1}^{n} \frac{1}{cK_i} [-\sin\theta] \Big|_{\theta_i}^{\theta_{i+1}}$$

$$= \pm 2 \sum_{i=1}^{n} \frac{1}{cK_i} [\sin\theta_i - \sin\theta_{i+1}]. \tag{39}$$

And since from Eqn. (10): $\cos\theta_i = cv_i$

$$R_n = \pm 2 \sum_{i=1}^{n} \frac{v_i}{K_i \cos\theta_i} [\sin\theta_i - \sin\theta_{i+1}]$$

and from Eqn. (8),

$$R_n = \pm 2 \sum_{i=1}^{n} \frac{1}{K_i} [v_i \tan\theta_i - v_{i+1} \frac{\sin\theta_{i+1}}{\cos\theta_{i+1}}]$$

$$= \pm 2 \sum_{i=1}^{n} \frac{1}{K_i} [v_i \tan\theta_i - v_{i+1} \tan\theta_{i+1}]. \quad (40)$$

Since this equation describes rays returning to the ground, then the angle, θ_{n+1}, grazing the top of layer n is zero,

$$\theta_{n+1} = 0$$

and only positive range is required, so:

$$R_n = 2\{\frac{v_n}{K_n} \tan\theta_n + \sum_{i=1}^{n-1} \frac{1}{K_i} [v_i \tan\theta_i - v_{i+1} \tan\theta_{i+1}]\}. \quad (41)$$

Equations (33) through (41) hold for $K_i \neq 0$. Generally, up to the ith layer, and if $K_i = 0$, and $i = m < n$, then from Eqn. (33):

$$R_n = 2\{[\sum_{i=1}^{m-1} x_i] + \frac{y_m}{\tan\theta_m} + [\sum_{m+1}^{n-1} x_i]\}. \quad (42)$$

The first term in Eqn. (42) is the range of the ray up to the mth layer as calculated by Eqn. (41), and the second term is the range in the mth layer calculated from trigonometry (Fig. 9). Equation (41) is used to add the third term to complete range calculations until the shot site level is reached. The number of terms is dictated by the number of non-adjacent zero velocity profiles.

Equation (42) is the general equation for the range of the acoustic wave in an n-layered atmosphere modified for $K_i = 0$. It is used to complement Eqn. (41) in the computer model REFFOCUS, described below in Section 4.

3.3 Time of Arrival

Again the time of arrival at the shot site level is twice the time to reach a turning point. According to Fermat's Law of least time - the time of passage of a ray between two fixed points is an extremum (minimum) with respect to possible paths connecting the points. The passage of sound rays of variable velocities through the atmosphere is governed by Fermat's law. This is true for any set of rays (at any angle θ) which connects two points such as the shot site and a focus, independent of the path length. The time of arrival, t_n, of a ray back at the height of the shot site is given by

$$t_n = 2 \sum_{i=1}^{n} \int_{h_i}^{h_{i+1}} \frac{dr}{v} \tag{43}$$

where: h_i = initial height in the ith atmospheric layer;
h_{i+1} = final height in the (i+1)th atmospheric layer;
dr = increment of radial displacement.

The Atmospheric layer thickness, y, is:

$$y = h_{i+1} - h_i.$$

The velocity, v, throughout the layer is:

$$v = v_i + K_i y.$$

Converting between polar and rectangular coordinates in 2-dimensions,

$$x = r \cos\theta \qquad y = r \sin\theta$$

$$dr = -\frac{dx}{\sin\theta} \qquad dr = \frac{dy}{\cos\theta}$$

(Note: The case for $K_i = 0$ will be examined later). For the case where $K_i \neq 0$:

$$t_n = 2 \sum_{i=1}^{n} \int_{h_i}^{h_{i+1}} \frac{(1/\sin\theta)dy}{v_i + K_i y} \tag{44}$$

where by geometry $\cos\theta = v_i + K_i y$

$$dy = -\frac{\sin\theta d\theta}{K_i}.$$

When $y = h_i$, $\theta = \theta_i$

$y = h_{i+1}$, $\theta = \theta_{i+1}$

we have

$$t_n = -2 \sum_{i=1}^{n} \frac{1}{K_i} \int_{\theta_i}^{\theta_{i+1}} \frac{d\theta}{\cos\theta} \quad . \tag{45}$$

Substitute: $u = \ln[\sec\theta + \tan\theta]$

So: $du = \dfrac{[\sec\theta \tan\theta + \sec^2\theta]d\theta}{[\sec\theta + \tan\theta]}$

$$= \frac{[1 + \sin\theta]}{[\cos\theta(1 + \sin\theta)]} d\theta$$

$$= \frac{d\theta}{\cos\theta} \quad .$$

Equation (45) thus becomes

$$t_n = -\sum_{i=1}^{n} \frac{2}{K_i} \int_{\theta_i}^{\theta_{i+1}} du \tag{46}$$

$$= -\sum_{i=1}^{n} \frac{2}{K_i} \ln[\sec\theta + \tan\theta] \Big|_{\theta_i}^{\theta_{i+1}} \tag{47}$$

$$= \sum_{i=1}^{n} \frac{2}{K_i} \ln\left[\frac{\sec\theta_i + \tan\theta_i}{[\sec\theta_{i+1} + \tan\theta_{i+1}]}\right] \quad . \tag{48}$$

Since this equation describes rays returning to the ground, then the angle, θ_{i+1}, grazing the top of layer n is zero, i.e.

$$\theta_{n+1} = 0.$$

So the time of arrival of a sound ray, back to shot site level is; from Eqn. (48),

$$t_n = 2\{\frac{1}{K_n} \ln[\sec\theta_n + \tan\theta_n] + \sum_{i=1}^{n-1} \frac{1}{K_i} \ln \frac{[\sec\theta_i + \tan\theta_i]}{[\sec\theta_{i+1} + \tan\theta_{i+1}]}\}. \tag{49}$$

Equations (43) through (49) hold for $K_i \neq 0$.

If $K_i = 0$, then by geometry, figure 9, for $i = m < n$,

$$\frac{t}{2} = \frac{y_m}{v_m \sin\theta_m} \quad .$$

Generally for n layers, if $K_i = 0$, and $i = m < n$, then:

$$t_n = 2\{t_m + \frac{y_m}{v_m \sin\theta_m} + (t_n - t_{m+1})\}. \quad (50)$$

The first term in Eqn. (50) gives the time for the ray to reach the mth layer using Eqn. (49), and the second term is the time to traverse the mth layer obtained from trigonometry. The last term is the additional time for the ray to reach shot site level as calculated using Eqn. (49). The number of terms is dictated by the number of non-adjacent zero velocity profiles.

Equation (50) is the general equation for the time of arrival of the acoustic wave in an n-layered atmosphere modified for $K_i = 0$. It is used to complement Eqn. (49) in the computer model REFFOCUS, described below in Section 4.

4. ACOUSTIC FOCUS PREDICTIONS

4.1 REFFOCUS - A Computerised Aid to Acoustic FOCI Modelling

REFFOCUS, in Fortran 77 code, is a computerised aid to predict the location of acoustic foci in the air by acoustic refraction. Using weather data, or velocity/height data it calculates, tabulates and, if appropriate, plots:

1. The maximum angle, θ_{1crit}, which will turn over in the atmosphere.
2. The range, R, of rays at discrete angles from $\theta = 0$ to θ_{1crit}.
3. The time of arrival, T, of these rays from $\theta = 0$ to θ_{1crit}.
4. The sound velocity/height profiles.
5. The ray path followed by each angle from $\theta=0$ to θ_{1crit}.
6. Multiple reflections of the Range, Time of arrival, and Ray paths for each angle from $\theta = 0$ to θ_{1crit}.

REFFOCUS is based on a model which does not attempt to use or model a real 3-dimensional atmosphere but rather a simplified, horizontally homogeneous and stable atmosphere without curvature or relief to produce a working model of focused sound rays. In accordance with the working model, overpressures developed either by direct, or by reflected sound ray convergence have not been attempted so that terrain and vegetation are not included in the model.

The program presently assumes:

1. Acoustic rather than shock wave behaviour over entire range.
2. Surface blasts or noise generation - not restricted to sea level.
3. A locally flat earth without curvature or relief.

4. **A horizontally homogeneous atmosphere where the weather conditions and sound velocities are stable.**

5. **Rays which return to earth at shot site level are reflected with 100% of their energy from the flat surface to return to earth at multiples of their initial range.**

REFFOCUS will be extended to -

1. Calculate approximate overpressures at the ranges of returned rays.

2. Tabulate all data, including weather data and overpressures.

3. Calculate and plot multiple azimuthal foci predictions so that a foci contour map is generated.

4. Calculate and plot the foci above ground which have observed on ray traces.

5. Calculate and plot foci from an above ground burst.

6. Be fully transportable to operate near location on an IBM or compatible personal computer.

REFFOCUS is designed to be readily used by an inexperienced person. To facilitate input there is the option of a keyboard or data file input; and a review option allows a recapitulation of data and graphs.

For each azimuthal sound velocity profile the three major equations used by REFFOCUS in the calculation of refracted rays through n layers of atmosphere are Eqns. (29), (41), (49).

Equation (29)

$$y = h_n - \frac{v_n}{K_n} \pm \sqrt{\frac{v_1^2}{(K_n \cos\theta_1)^2} - (x - \{[\sum_{i=1}^{n-1} x_i] + X_n\})^2}$$

calculates the y cartesian coordinate with respect to displacement of the ray in the x direction until turnover (at $x = x_{max}$). REFFOCUS produces an extra set of cartesian coordinates by reflection about x_{max} so that the ray's trajectory is completed from the shot site - to turnover - to ground.

Equation (41)

$$R_n = 2\{\frac{v_n}{K_n} \tan\theta_n + \sum_{i=1}^{n-1} \frac{1}{K_i} [v_i \tan\theta_i - v_i - 1 \tan\theta_{i+1}]\}$$

calculates the range for each ray with angle $\theta = 0$ to θ_{crit}. Although x coordinate calculations are from the shot site to turnover, the range of each ray is simply twice x_{max}.

Equation (49)

$$t_n = 2\{\frac{1}{K_n} \ln[\sec\theta_n + \tan\theta_n] + \sum_{i=1}^{n-1} \frac{1}{K_i} \ln[\frac{\sec\theta_i + \tan\theta_i}{\sec\theta_{i+1} + \tan\theta_{i+1}}]\}$$

calculates the time of arrival of each ray with angle $\theta = 0$ to θ_{1crit}. The total time for the ray to return to ground is twice that of the time to turnover.

Range, Time of arrival, and Ray trace coordinate are modified when $K_i = 0$ as discussed in sections 3.1.5, Eqn. (31); 3.2, Eqn. (42); 3.3, Eqn. (50).

4.2 Typical Velocity Profiles

Figures 10 to 17c have been produced by REFFOCUS to illustrate the capabilities of the program and to show some velocity profiles considered relevant for a ground explosion. These figures are in addition to those simple profiles shown in figures 2 to 4. With the exception of figures 10 and 17a, b, c the graphs are in groups of four, each with the same figure number and with letters a, b, c or d. The nomenclature is as follows:

a) Sound velocity profile
b) Range vs initial ray angle
c) Time of arrival of sound ray vs initial ray angle
d) Ray traces

Type 1 (Fig. 10)

No. of layers = 4

h_i = 0 m	v_1 = 340 m/s	
h_2 = 500 m	v_2 = 335 m/s	$K_1 = -0.01\ s^{-1}$
h_3 = 750 m	v_3 = 340 m/s	$K_2 = 0.02\ s^{-1}$
h_4 = 1250 m	v_4 = 335 m/s	$K_3 = -0.01\ s^{-1}$

Figure 10 shows a velocity profile where the sound velocity never exceeds that at ground level. This is in spite of a positive velocity gradient between 500 and 750 metres. In this case REFFOCUS will not generate range, time, or ray trace graphs because no ray will return to the ground. A focus is not possible.

Type 2 (Figures 11a, b, c, ed)

No. of layers = 4

h_1 = 0 m	v_1 = 340 m/s	
h_2 = 500 m	v_2 = 335 m/s	$K_1 = -0.01\ s^{-1}$
h_3 = 750 m	v_3 = 345 m/s	$K_2 = 0.04\ s^{-1}$
h_4 = 1250 m	v_4 = 340 m/s	$K_3 = -0.01\ s^{-1}$

Figure 11a shows a velocity profile where there is initially a negative velocity gradient followed by a positive gradient. This would probably arise due to a temperature inversion, but could also be a result of wind shear. Low angle rays which turn over before the top of the second atmospheric layer will be able to return to the ground. This is possible because sound velocities at heights between 625 to 750 metres are greater than the 340 m/s at the shot site. Higher angle rays will not return because of the negative gradient above 750 metres.

The maximum or critical angle, below which rays may be allowed to return to the ground, is 9.77^{o} in figure 11b. At low angles there can be a large change in the final range between each angle. This is shown as a large slope. Conversely, near the critical angle, θ_{1crit}, the slope of the curve is nearly zero which means rays of different angles are tending to converge upon a focus.

As is generally the case, the time of arrival of each ray has a graph identical to the range graph except for the units of measurement. According to Fermat's law these graphs will show the same turning points - maxima, minima, and points of inflection. By necessity, these turning points control and restrict the shape of these two curves so that they are usually identical - except when there is a single positive velocity gradient as in figures 16b, c. Because of this, it can be seen that the time of travel of a ray increases with range in all cases.

Figure 11d is the ray trace. At ground level there is a relative convergence of rays between 9^{o} to 9.77^{o} at a range of about 9 km. Rays at angles greater than $\theta_{1crit} = 9.77^{o}$ do not turn over and do not return to the ground. These rays are not shown on any ray trace by REFFOCUS. Significantly, there may be a possible focus between 525 to 600 m altitude. This is not a ground range, and as such is not considered in the previous graphs. The region where there are no returned rays from 0 to 9 km is referred to as a quiet zone.

Type 3 (Figures 12a, b, c, d)

No. of layers = 4

$h_1 = 0$ m	$v_1 = 340$ m/s	
$h_2 = 500$ m	$v_2 = 340$ m/s	$K_1 = 0\ s^{-1}$
$h_3 = 750$ m	$v_3 = 350$ m/s	$K_2 = 0.04\ s^{-1}$
$h_4 = 1250$ m	$v_4 = 350$ m/s	$K_3 = 0\ s^{-1}$

There are two zero velocity gradients in figure 12a with a positive gradient in between. To allow REFFOCUS to produce range, time and ray trace graphs the first velocity gradient was made slightly negative and approaching zero. Any rays greater than 13.73^{o} in figures 12b, c will travel into the third atmospheric layer starting at 750 m and are refracted upward. These rays do not return to the ground and so cannot be represented in figures 12b, c and are not represented in figure 12d. Because of the first zero gradient, rays propagating at low angles will radiate radially and low to the ground for nearly infinite distances. For this reason REFFOCUS allows the selection of graphical range and height limits to elucidate details of ray propagation nearer the shot site. The rays will begin to turn over in the second layer at a relatively large range from the shot site. Figures 12b, c show that these very low angle rays produce large ranges and times of arrival with very little chance of a focus. The graphs only produce a zero gradient near θ_{1crit} where a spread of rays converge to produce a possible focus. This is more easily seen in figure 12d.

The larger ranges produced by the long radial trajectories of low angle rays are seen in figure 12d. Larger angle rays converge toward the 8 km range. The ray trace

graph was also rescaled to limit graphed ranges to 20 km. Again there appears to be a concentration of rays in the atmosphere at a height of 250 to 500 m.

Type 4 (Figures 13a, b, c, d)

No. of layers = 5

h_1 = 0 m	v_1 = 340 m/s	
h_2 = 500 m	v_2 = 342 m/s	$K_1 = 0.004\ s^{-1}$
h_3 = 650 m	v_3 = 355 m/s	$K_2 = 0.020\ s^{-1}$
h_4 = 1150 m	v_4 = 357 m/s	$K_3 = 0.004\ s^{-1}$
h_5 = 1250 m	v_5 = 357 m/s	$K_4 = 0\ s^{-1}$

There are three positive velocity gradients in figure 13a up to 1150 m, capped by a uniform velocity above it. The central large velocity gradient can be expected to sharply refract any rays which enter the thin atmospheric layer. Figures 13b, c show that very low angle rays are allowed to propagate small distances in the first layer whilst being immediately refracted downward. As ray angles increase, the rays are allowed to travel relatively large distances before turnover just within the first layer. Thereafter, ray angles allow propagation into the second layer and, as the critical angle for the second atmospheric layer is approached (about 15^{o}), the rays are provided a more refractive medium and are quickly turned over to return to ground at small ranges and low time intervals. These rays converge toward a possible focus at about 5.5 km shown by the flat region in figures 13b, c and clearly in figure 13d. Discontinuities at this point and at the boundary of other layers would be less sharp if smaller angle increments were to be used in the calculation. The two apparent discontinuities are in fact the maximum and minimum of the range and time graphs.

Figure 13d shows the increase, decrease, then increase in range described by the previous graphs. There is a rapid increase in range at low angles, then the decrease in range as rays are refracted within the second layer and the final rapid increase in range as the larger rays near θ_{1crit} are slowly turned over in the third layer. Rays of still greater angle are refracted upward, never to return to the ground, and are not shown in figure 13d.

Type 5 (Figures 14a, b, c, d)

No of layers = 4

h_1 = 0 m	v_1 = 340 m/s	
h_2 = 500 m	v_2 = 345 m/s	$K_1 = 0.01\ s^{-1}$
h_3 = 750 m	v_3 = 335 m/s	$K_2 = -0.04\ s^{-1}$
h_4 = 1250 m	v_4 = 340 m/s	$K_3 = 0.01\ s^{-1}$

There is only one atmospheric layer of interest in figure 14a. Any ray which has not turned over by the top of the first layer will be refracted upward by the following inversion-like layer and cannot be completely refracted toward the ground by the third layer of positive gradient. The third layer does not produce sound velocities greater than that found at the top of the first layer and so does not contribute toward sound focusing at the ground.

Because we are essentially considering only a single atmospheric layer limited to 500 m, figures 14b, c show an almost linear increase in range and time of arrival with ray angle up to $\theta_{1crit} = 9.77^{o}$. All of these rays are turned over within the 500 m ceiling. Although there is no focus possible the sound levels along the specified direction

are higher than those expected when acoustic refraction is not considered. The range is limited to 11.7 km and the corresponding time to 34.26 s, by the inversion-like layer above 500 m.

Type 6 (Figures 15a, b, c, d)

No. of layers = 5

h_1 = 0 m	v_1 = 340 m/s	
h_2 = 500 m	v_2 = 346 m/s	K_1 = 0.012 s^{-1}
h_3 = 650 m	v_3 = 340 m/s	K_2 = -0.040 s^{-1}
h_4 = 1400 m	v_4 = 349 m/s	K_3 = 0.012 s^{-1}
h_5 = 1500 m	v_5 = 349 m/s	K_4 = 0 s^{-1}

The atmospheric conditions in figure 15a are very similar to Type 5 excepting the final velocity gradient is extended higher so that there exist sound velocities greater than in lower layers. Rays turning over are limited to 1400 m where the last velocity gradient is zero.

Figs. 15b, c are similar again to those of Type 5 up to the critical angle of 9.77° for the first layer. Larger angle rays travel into the second layer and are refracted upward (Fig. 15d) and may be turned over in the third layer between 1250 and 1400 m. These rays travel large distances in the second layer and some rays with angles close to θ_{1crit} do turn over before some lower angle rays. There is a near focus for those angles near θ_{1crit} at a range of 20 km.

The ray trace below 500 m (the first layer) is identical to Type 5 with the addition of returned rays which turn over between 1250 to 1400 m heights. Some rays have converged to a range of around 20 km. There is a quiet zone between 10 and 20 km since no rays have turned over in the second layer.

Type 7 (Figures 16a, b, c, d)

No. of layers = 2

h_1 = 0 m	v_1 = 340 m/s	
k_2 = 500 m	v_2 = 345 m/s	K_1 = 0.010 s^{-1}

Figure 16a has the single positive velocity gradient seen in figure 4. Because the shape of the graphs in figures 16b, c are restricted only by the one turning point at 0° they are not identical but there is still the asymptotic rise in range and time of arrival near θ_{crit}. Figure 16d appears similar to that of Type 5 because there is only one atmospheric layer of interest with a positive velocity gradient. Again these graphs may be viewed by choosing more reasonable range, time and height graphing limits.

As in Type 5, sound levels are enhanced in the near-medium fields over those from direct ray traverse.

Type 8 (Figures 17a, b, c)

No. of layers = 5

$h_1 = 0$ m	$v_1 = 340$ m/s	
$h_2 = 500$ m	$v_2 = 342$ m/s	$K_1 = 0.004\ s^{-1}$
$h_3 = 650$ m	$v_3 = 355$ m/s	$K_2 = 0.02\ s^{-1}$
$h = 1150$ m	$v_4 = 357$ m/s	$K_3 = 0.004\ s^{-1}$
$h_5^4 = 1250$ m	$v_5 = 357$ m/s	$K_4 = 0\ s^{-1}$

These graphs have been generated by REFFOCUS from the velocity profile of Type 4 with one reflection at the ground of the returned rays. Reflected rays may be identified in both the Range and Time of Arrival graphs by their relative amplitudes in range or time with respect to the unreflected rays. The first reflected sets of rays have twice the range and time of their first return to the ground. The second reflection has three times the range and time, and so on. Focii may experience constructive interference when rays of a different number of reflections are incident at a common range and time of arrival. Figures 17a, b show that there may be another focus derived from the reflection of the first focus. Subsequent foci may be less intense compared to the original focus. This may be shown by the shorter flat sections corresponding to reflected rays of $\theta \approx 16^{\circ}$ which turn over just within the second layer in figures 17a, b. However, other rays may converge onto the reflected focus, e.g. the unreflected rays with angles 4° and 7°.

Figure 17c shows the ray trace of both the unreflected and reflected rays. Again each reflected ray may be identified by its larger range than the corresponding unreflected ray. Also the arc of a reflected ray describes exactly the arc of an unreflected ray, beginning at the return to ground of the unreflected ray. A number of possible foci may be inferred using this graph and the range vs θ plot. These occur at ranges of 5.4 and 10.8 km, and at 15 km. The first two ranges correspond to the critical angle in the first layer. The ray trace could be reproduced with a lower range limit so that foci may be examined more closely. Additionally further reflections may be graphed by REFFOCUS.

5. CONCLUSION

Installations which produce noise require a method to estimate the unusual propagation of noise over long distances with anomalously large intensity. The blast scaling principle by charge weights may often produce gross errors in the estimation of overpressures at significant distances from a shot site, the principle ignores weather conditions and assumes a homogeneous atmosphere. Weather conditions may cause variations in the velocity of sound which allows the atmosphere to refract sound waves and act as an acoustic lens. Certain weather conditions such as temperature inversions may allow an acoustic focus many kilometres away from a shot site.

Acoustic propagation from a noise producing installation has been mathematically modelled to assist in the prediction of anomalous overpressures by acoustic focusing. Additionally, MRL, has developed a computer model, REFFOCUS, to illustrate foci in a vertically inhomogeneous, non-turbulent, moving atmosphere. The model is produced from sound velocity profiles derived primarily from temperature and wind shear profiles.

The results obtained have shown that the combined examination of Range versus θ and Ray trace plots for a given set of weather conditions may be enough to infer

the possibility of a focus by purely graphical means. This can be achieved by considering the angular spread of rays converging down range from the shot site. Acoustic foci may be predicted by the collaborated observation of:

1. a zero slope in the Range versus θ plot and,

2. the relative density of rays at the convergence of rays back to the ground in the Ray trace plot.

Although overpressures are not estimated in this model the contribution of each energy tube, containing an angular spread of rays incident at a common range and time, could be used to calculate the concentration of the sound wave energies at a focus and then related to overpressure. In this fashion, those installations which produce noise or potentially shocked acoustic foci at extended ranges may base the decision to proceed according to REFFOCUS predictions using the prevailing weather data. REFFOCUS can therefore be used to minimise noise and larger overpressures and can be extended to confirm atmospheric weather data.

Presently atmospheric data may be entered into the computer model, REFFOCUS, in the form of stratified sound velocity data. Alternatively, simple trigonometric relations for the wind velocity components, and temperature affected sound velocity components has been included in the REFFOCUS code to directly process weather data. Using these data options the velocity profiles, K_i, between each set of weather measurements are calculated and the full sound velocity profile, Range versus θ, Time of arrival of sound rays versus θ, and Ray traces may be plotted.

This acoustic focus model assumes noise generation in a vertically inhomogeneous atmosphere with stable weather and sound velocities at ambient pressure. In order to produce a working acoustic foci model we have not considered the earth curvature, relief, atmospheric composition, blast weights, and sonic attenuation.

This model of acoustic refraction in the atmosphere, and REFFOCUS, completes Stage 1 of the acoustic focused event predictions. Stage 2 will be used to experimentally verify predictions derived from REFFOCUS.

6. ACKNOWLEDGEMENTS

I am grateful to Dr P. Ryan, Materials Research Laboratory, for his computer plotting subroutine which is used by REFFOCUS to model foci. Similarly, I would like to thank D. Oliver, R. Borg and R. Kummer for their useful suggestions.

7. REFERENCES

1. Baker, W.E. (1973). Explosions in air. University of Texas Press, Austin & London.

2. Berning, W. (1948). Investigation of the propagation of blast waves over relatively large distances and the damaging possibilities of such propagation (BRL Report No 675). Aberdeen Proving Ground: Ballistics Research Laboratory.

3. Braddick, H.J.J. (1965). Vibrations, waves and diffraction. London: McGraw-Hill Pub. Co. Ltd.

4. Cox, E.F., Plagge, H.J. and Reed, J.W. (1952). Damaging air shocks at large distances from explosions. Sandia Corporation.

5. Herman, R.A., Wessels and Carel A. Velds (1983). Sound propagation in the surface layer of the atmosphere. Journal of the Acoustical Society of America, 74 (1).

6. Kahler, J.P. (1979). Focus - A computerised aid for making sound propagation forecasts (Report No. ADTC-TR 79-8). Hollman AFB: Staff Meteorology 6585th Test Group.

7. Perkins, B., Lorrain, P.H. and Townsend, W.H. (1960). Forecasting the focus of air blasts due to meteorological conditions in the lower atmosphere (Report No. 1118). Aberdeen Proving Ground: Ballistics Research Laboratory.

8. Reed, J.W. (1969). Acoustic wave effects project: airblast prediction techniques, Albuquerque: Sandia National Laboratories, Test Effects Dept. 9150.

9. Reed, J.W. (1985). Damaging distant airblast from minor scale. Albuquerque: Sandia National Laboratories, Ground Motion and Seismic Division - 7111.

10. Reed, J.W. Climatological assessment of explosion airblast propagations. Albuquerque: Sandia National Laboratories, Ground Motion & Seismic Division - 7111.

11. Sach, C.I. (1961). Long range blast pressure prediction (MRL Technical Note MRL-TN-59). Maribyrnong, Vic.: Materials Research Laboratory.

12. Sills, A.G. (1982). The prediction of sound intensity from an explosive source. Applied Acoustics, 15, 231-240.

13. Weinstock, R. (1952). International series in pure and applied calculus of variations. New York: McGraw-Hill Book Co. Inc.

14. Whitham, G.B. (1957). A new approach to problems of shock dynamics. Part 1: Two-dimensional problems. Journal of Fluid Mechanics, 2, 145-71.

GLOSSARY OF SYMBOLS

n	Number of atmospheric layers
i	Subscript i=1,2,3,....,m refers to the ith layer where m≤n
v	Velocity of sound in air
γ	Cp/Cv=ratio of specific heats at constant pressure and temperature in dry air
R	Specific gas constant in dry air = 287.05 (J kg^{-1} K^{-1})
T	Gas temperature (K)
q	Specific humidity (kg/kg of moist air)
ρ	Density of an acoustic medium
Z	Acoustic Impedance
Z_1	Acoustic Impedance of the first acoustic medium
Z_2	Acoustic Impedance of the second acoustic medium
E_R	The fraction of energy reflected across an acoustic boundary
E_T	The fraction of energy transmitted across an acoustic boundary
K	Velocity profile (=dv/dy) of layer i
V_i	Sound velocity at the foot of layer i
v_{i+1}	Sound velocity at the top of a sound ray in the ith layer or at the foot of the (i+1)th layer
t	Time
δt	Increment in time
θ	Angular displacement from the horizontal
y	Vertical displacement from the shot site
x	Horizontal displacement from the shot site
y'	Derivative of y, with respect to x
y"	Second derivative of y, with respect to x
θ_i	Initial angular displacement from the horizontal in the ith layer

θ_{i+1}	Initial angular displacement from the horizontal in the (i+1)th layer, OR final angular displacement from the horizontal at the top of a sound ray in the ith layer
θ_{1crit}	Maximum angular displacement from the horizontal at the shot site which will produce a grazing ray at the top of the (i-1)th layer
h_i	Initial height at the origin of the ray in the ith layer
h_{i+1}	Final height of the ray in the ith layer, OR the initial height of the ray in the (i+1)th layer
y_i	Vertical displacement of the ray in the ith layer
x_i	Horizontal displacement of the ray, from the origin of the ray in the ith layer before turnover
X_i	Horizontal displacement of the centre of the circle from the origin of the ray in the ith layer
R_n	Range (horizontal) of a ray in n layer
t_n	Time of arrival of a ray back to the shot site height in n layer
r	Radial displacement
dr	Increment of radial displacement

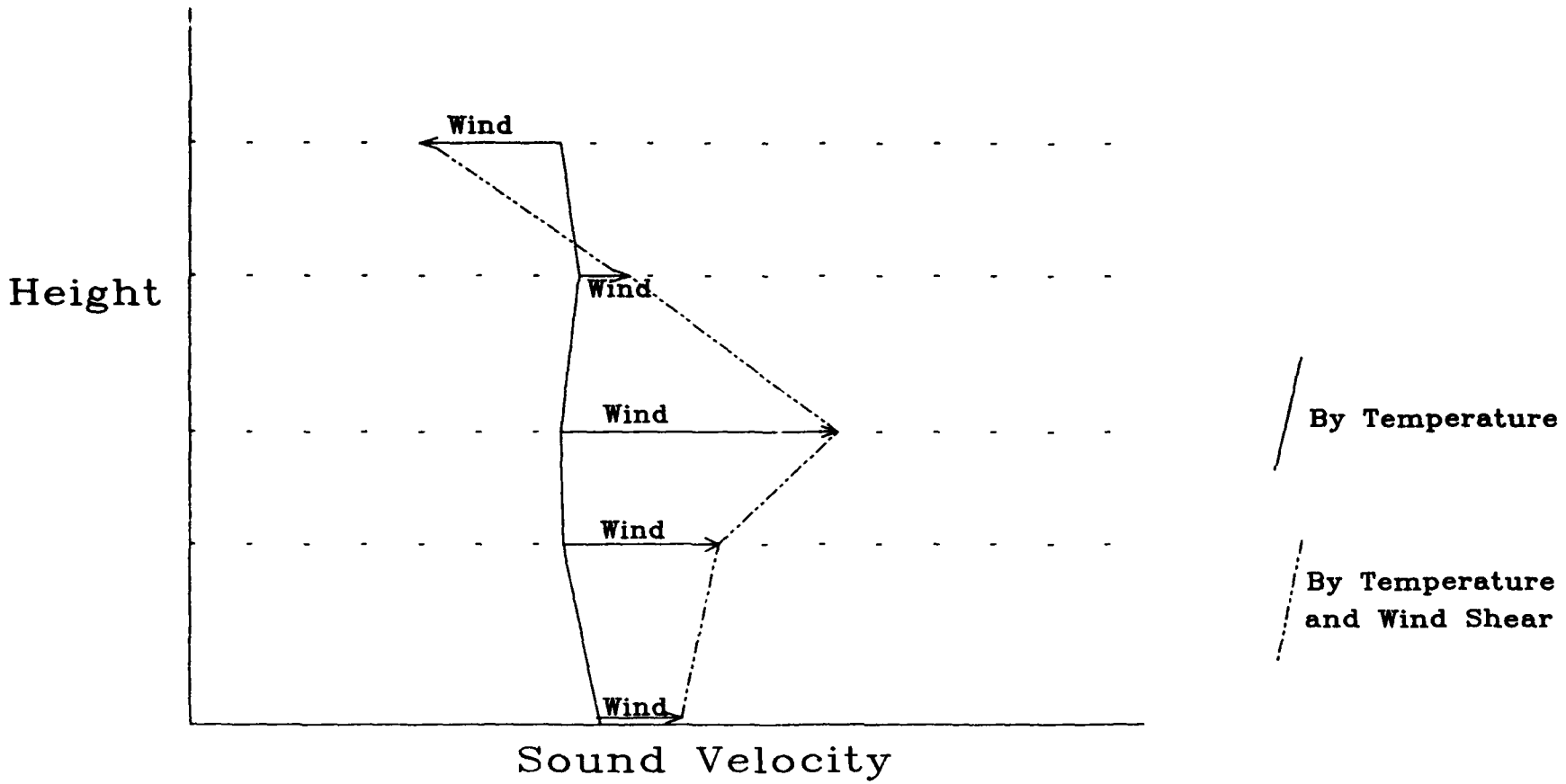

FIGURE 1 Temperature and Wind Shear Effects On Sound Velocity Profiles

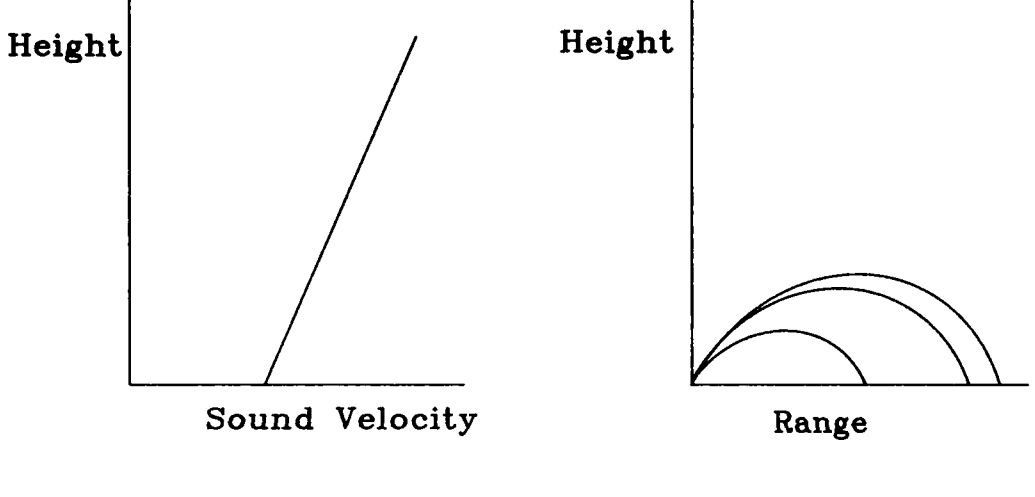

FIGURE 2 Basic Velocity Profile K>0

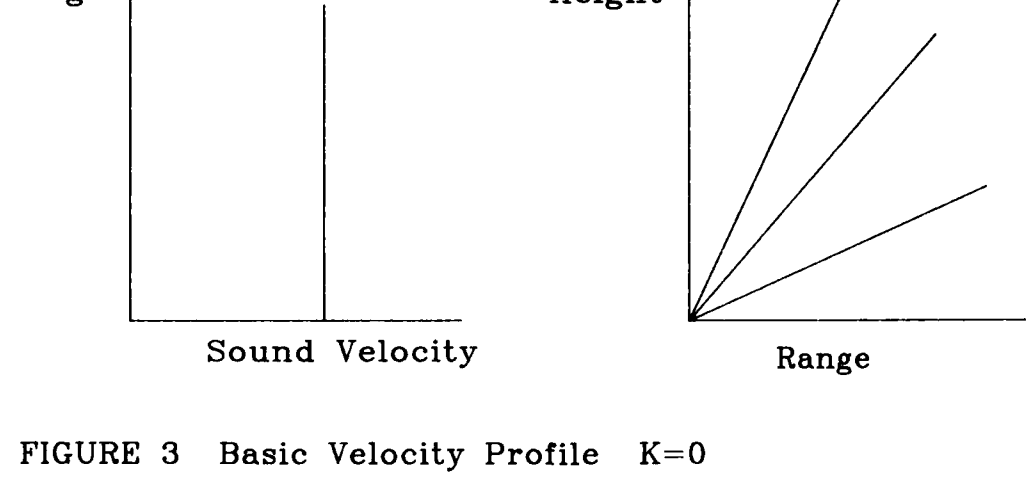

FIGURE 3 Basic Velocity Profile K=0

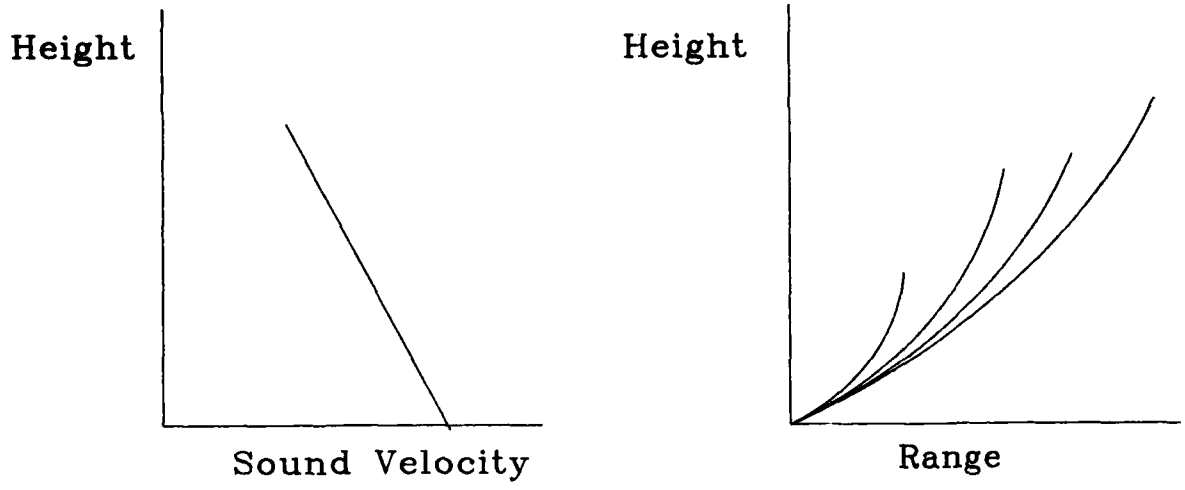

FIGURE 4 Basic Velocity Profile $K<0$

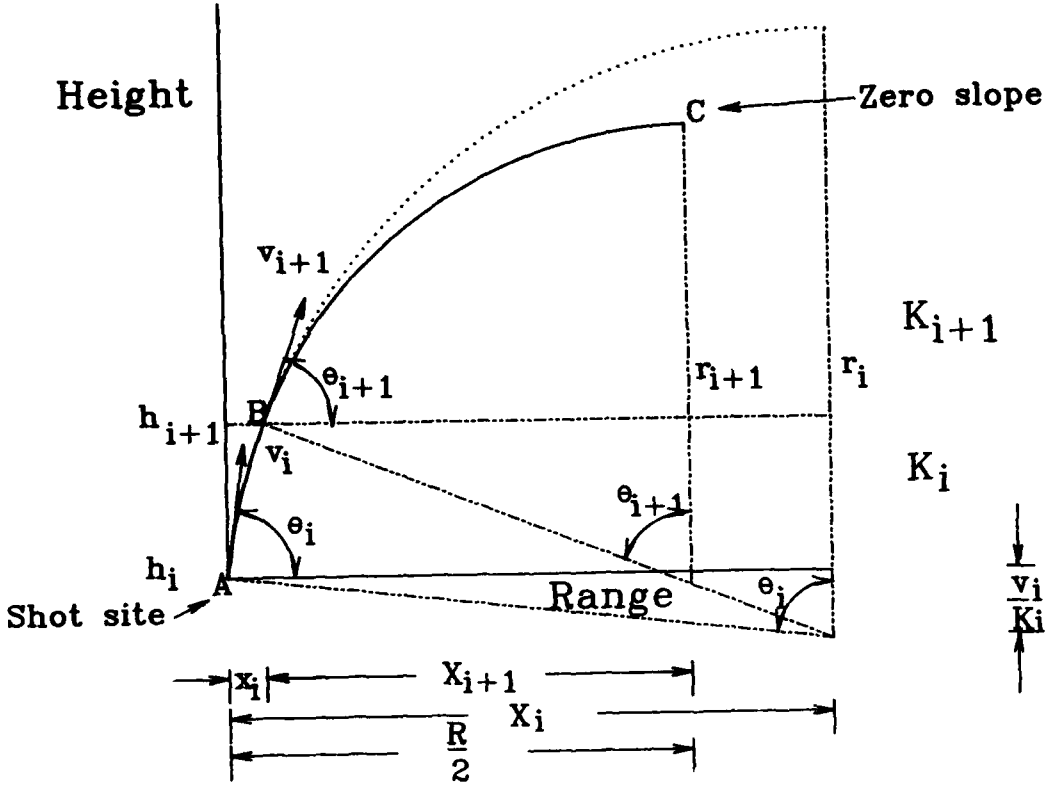

FIGURE 5A 2 Atmospheric Layers
With Positive Sound Velocity Profiles

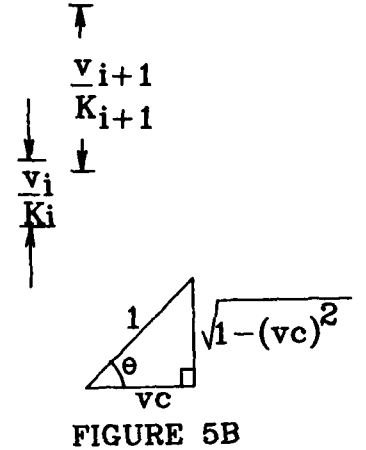

FIGURE 5B
Trigonometric Relation

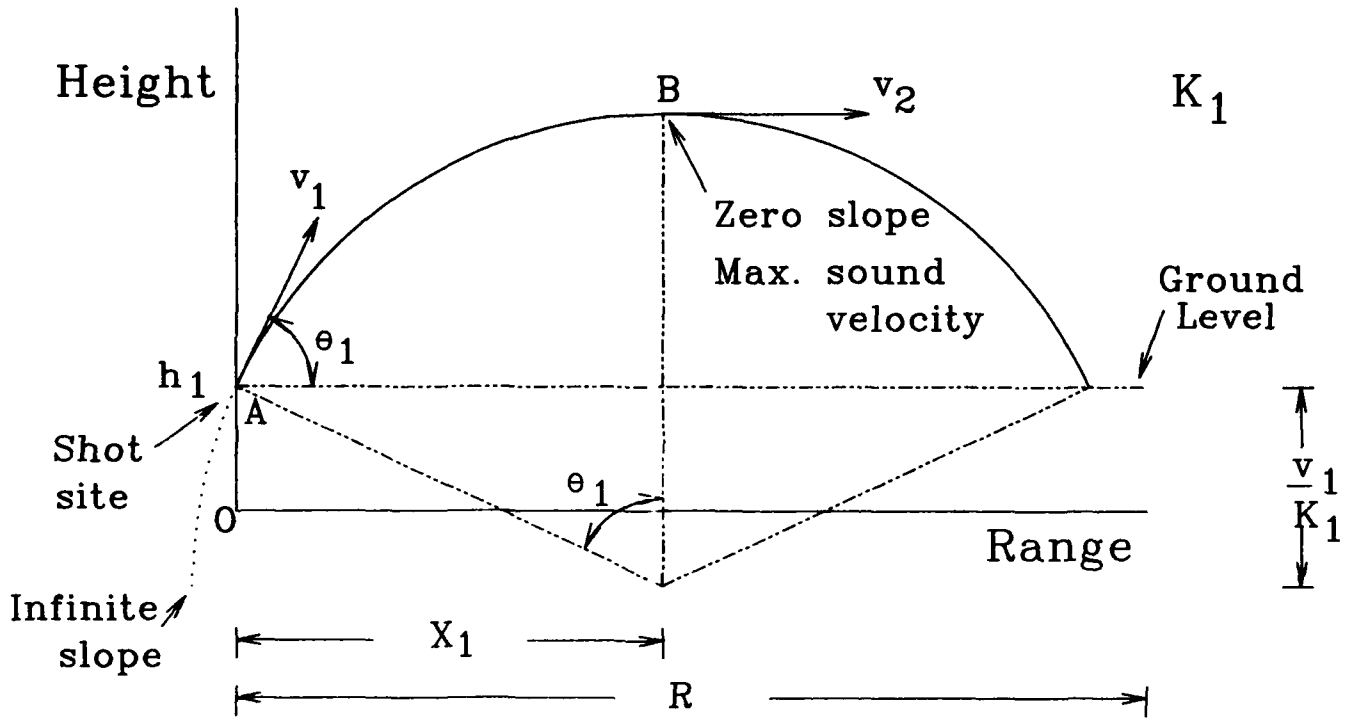

FIGURE 6A 1 Atmospheric Layer
With A Positive Sound Velocity Profile

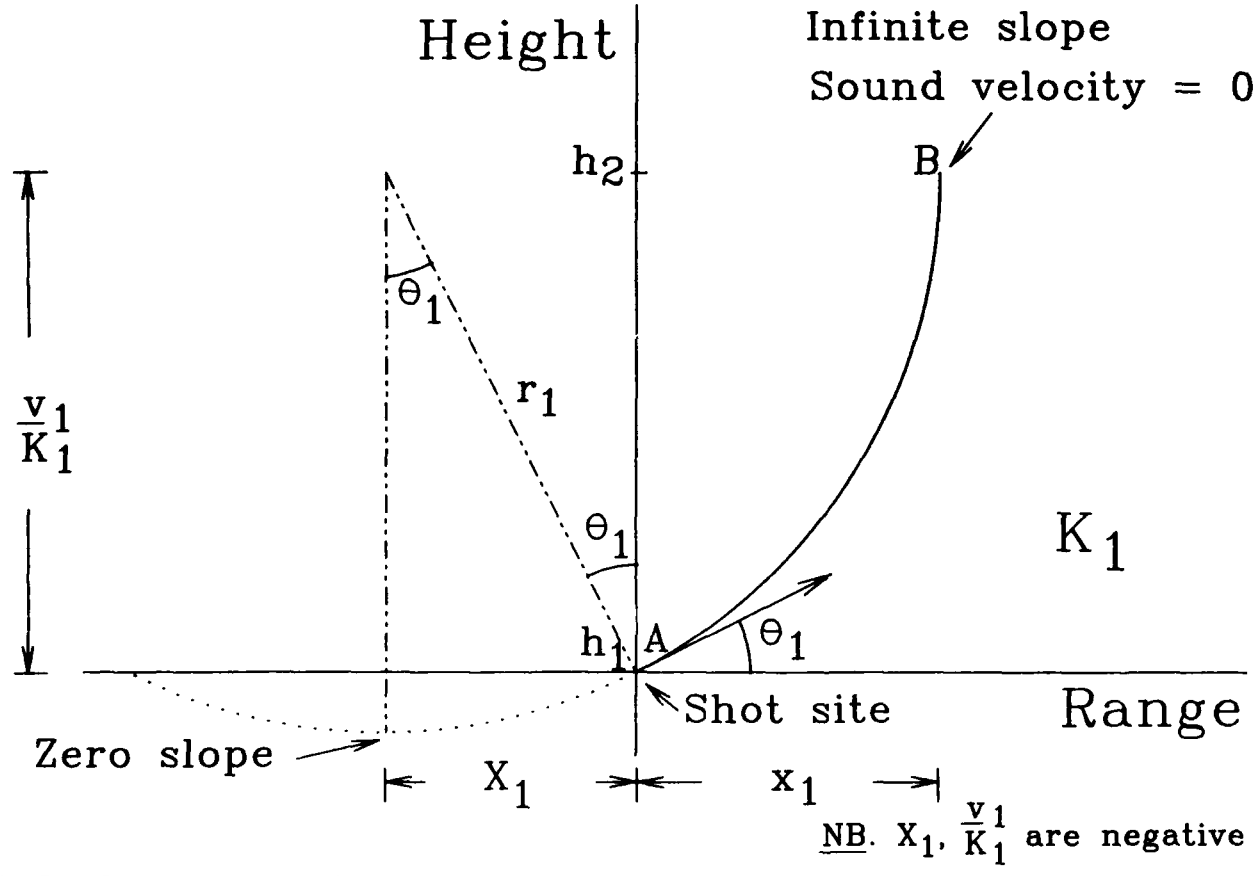

FIGURE 6B 1 Atmospheric Layer
With A Negative Sound Velocity Profile

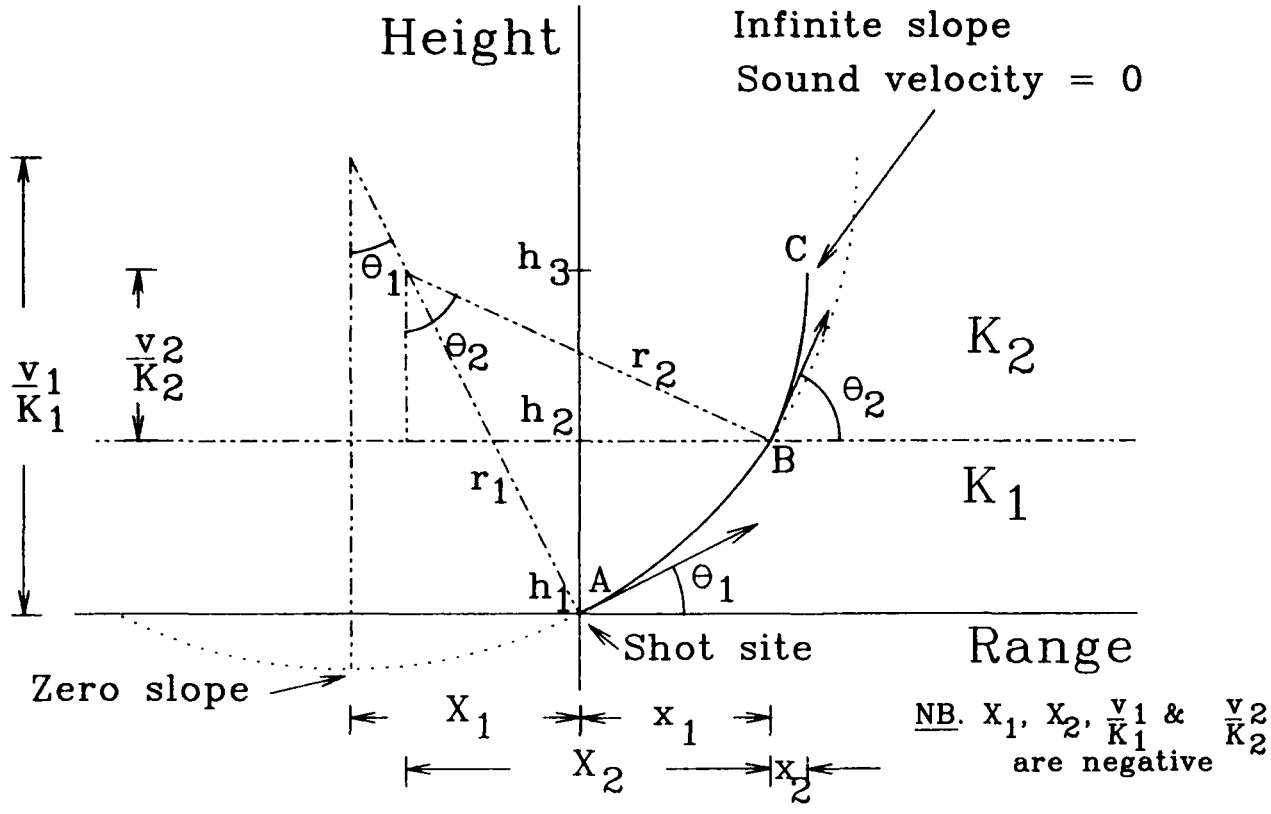

FIGURE 7 2 Atmospheric Layers
With A Negative Sound Velocity Profile

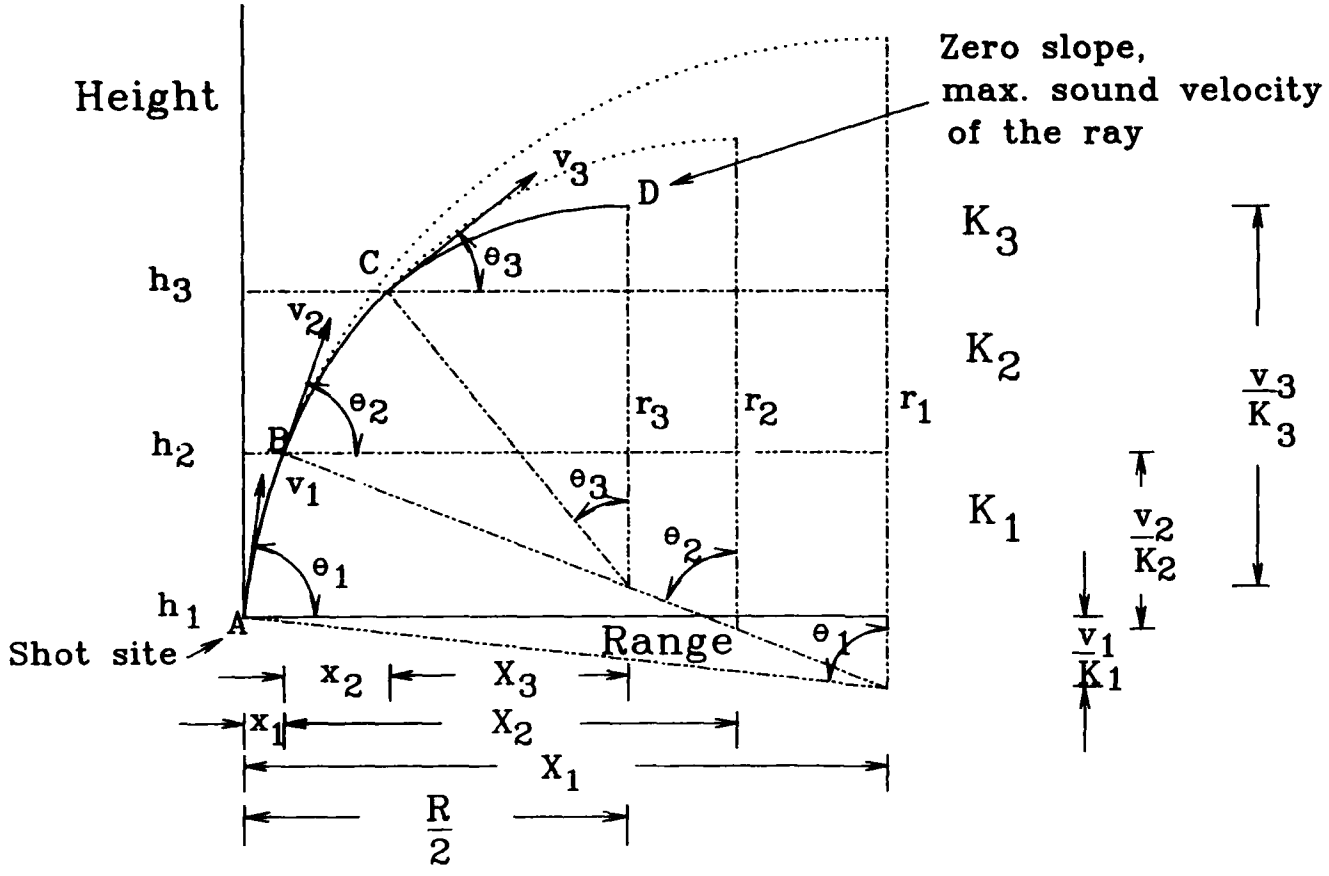

FIGURE 8 3 Atmospheric Layers
With Positive Sound Velocity Profiles

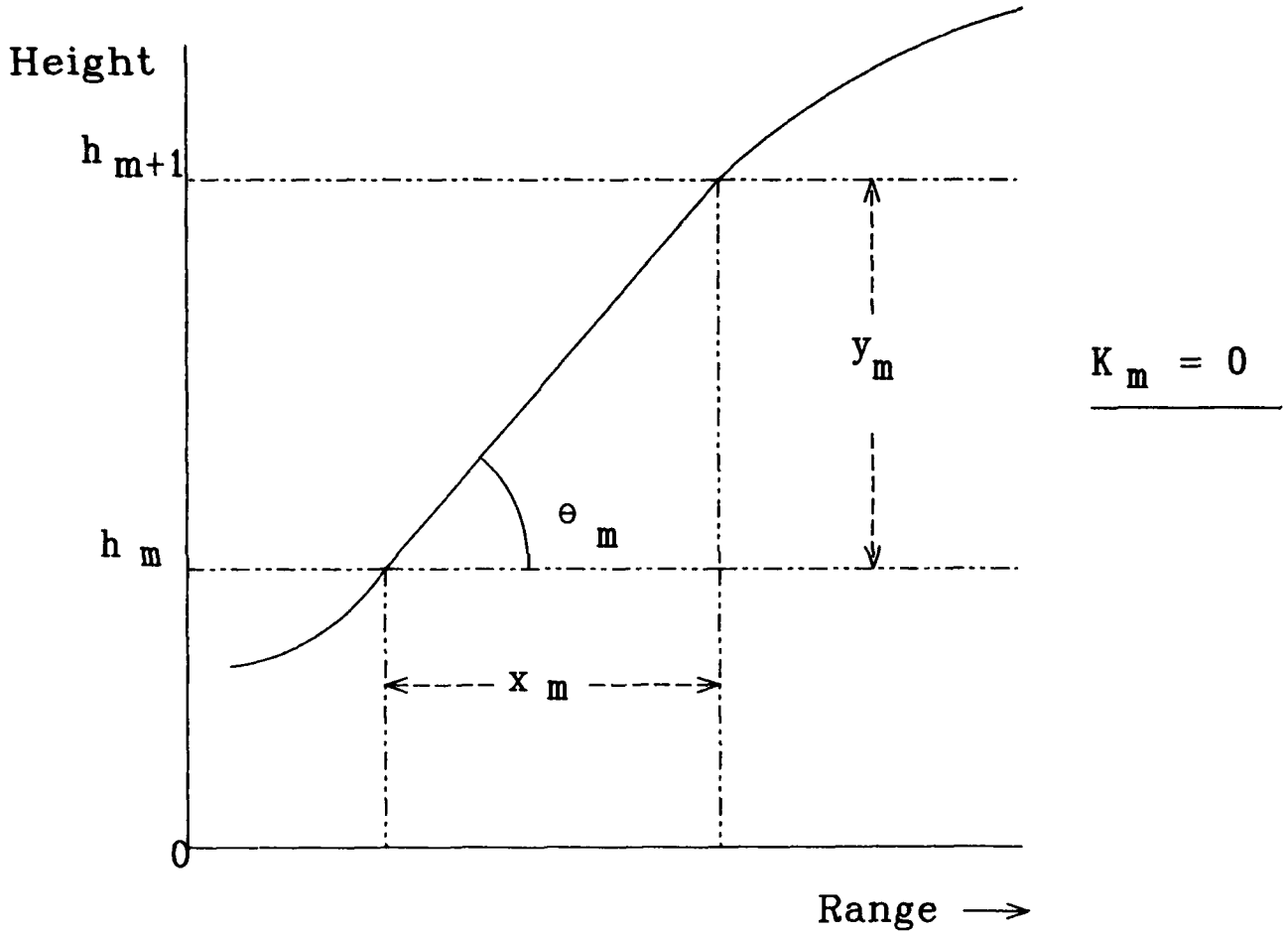

FIGURE 9 An Atmospheric Layer With A Zero Sound Velocity Profile

Figures 10–17 have been produced using REFFOCUS to illustrate the capabilities of the program and to show some velocity profiles considered relevant for a ground explosion.

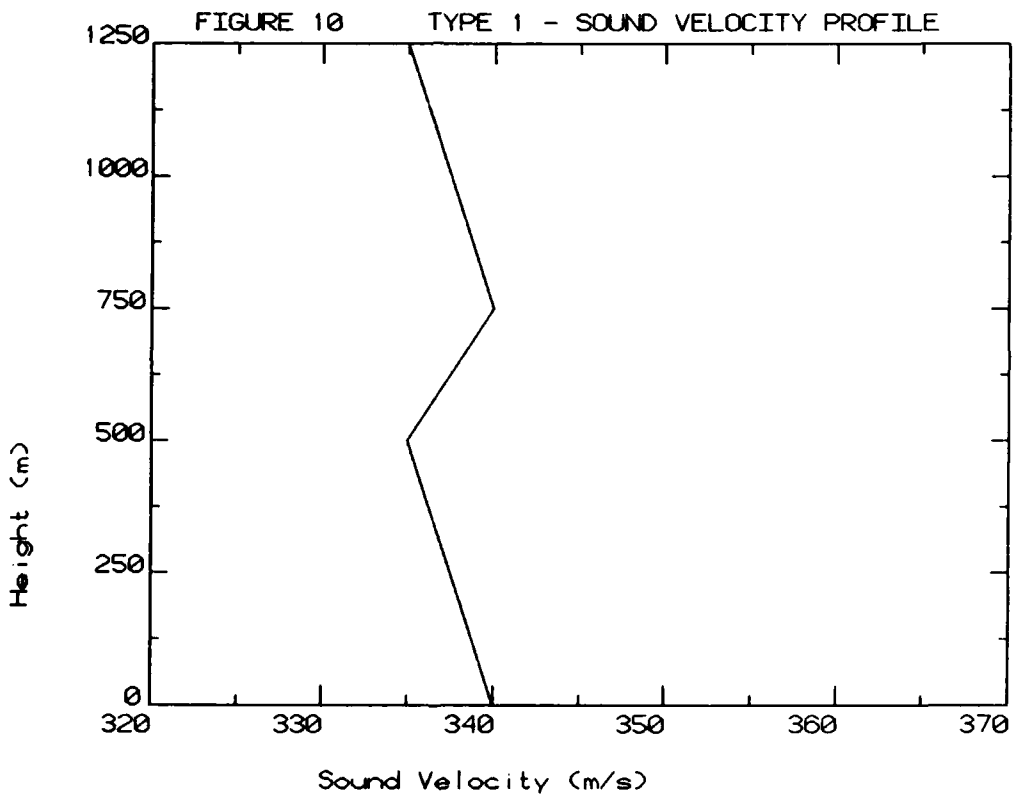
FIGURE 10 TYPE 1 - SOUND VELOCITY PROFILE
1250
1000
750
500
250
0
Height (m)
320
330
340
350
360
370
Sound Velocity (m/s)

FIGURE 11A TYPE 2 - SOUND VELOCITY PROFILE

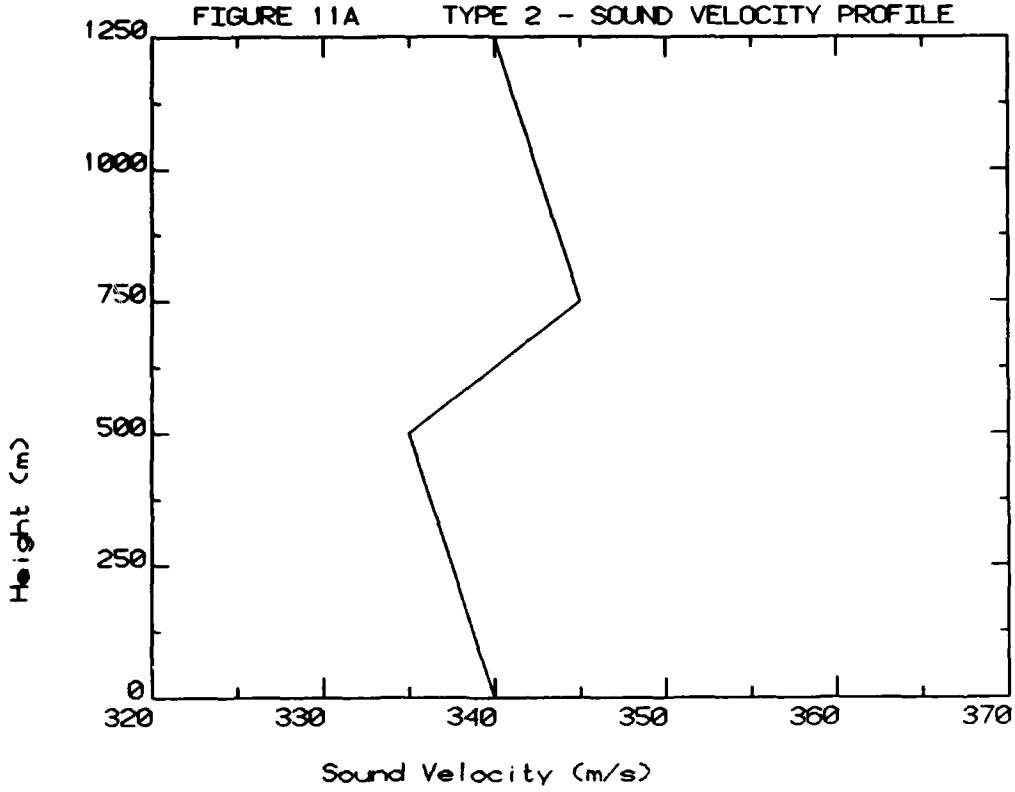

FIGURE 11B TYPE 2 - RANGE vs ELEVATION ANGLE

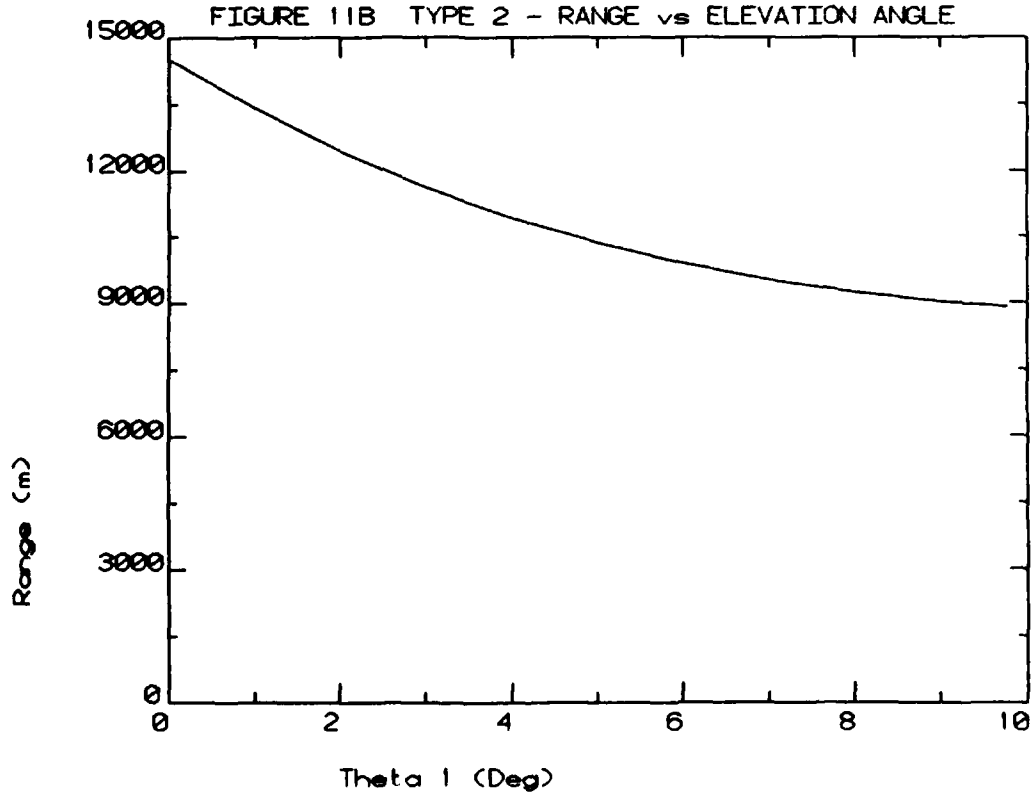

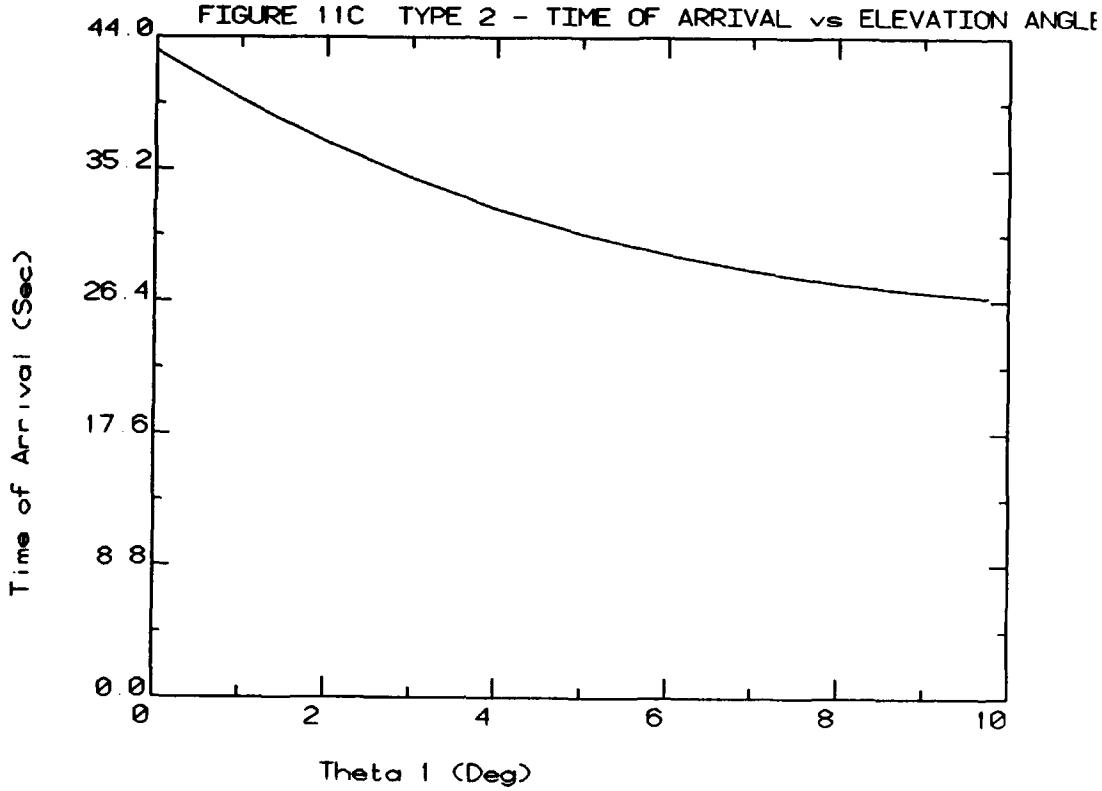
FIGURE 11C TYPE 2 - TIME OF ARRIVAL vs ELEVATION ANGLE
44.0
35.2
26.4
17.6
8.8
0.0
Time of Arrival (Sec)
0
2
4
6
8
10
Theta 1 (Deg)

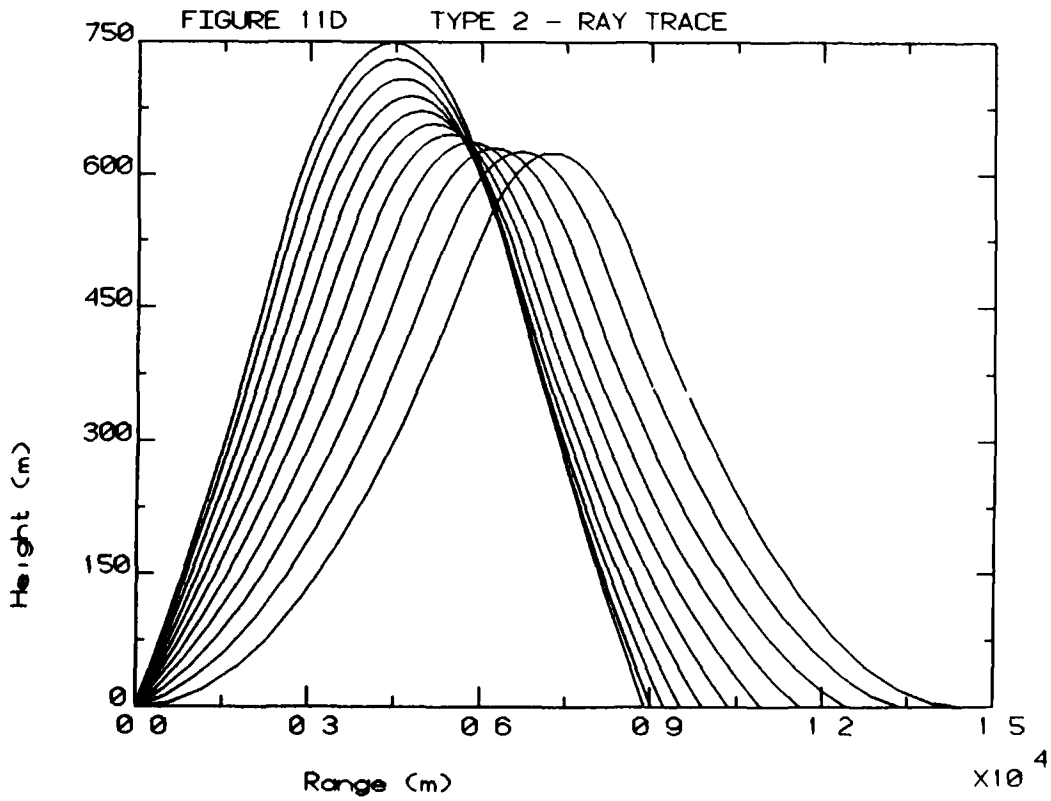
FIGURE 11D TYPE 2 - RAY TRACE
750
600
450
300
150
0
Height (m)
0.0
0.3
0.6
0.9
1.2
1.5
Range (m)
X10 4

FIGURE 12A TYPE 3 - SOUND VELOCITY PROFILE

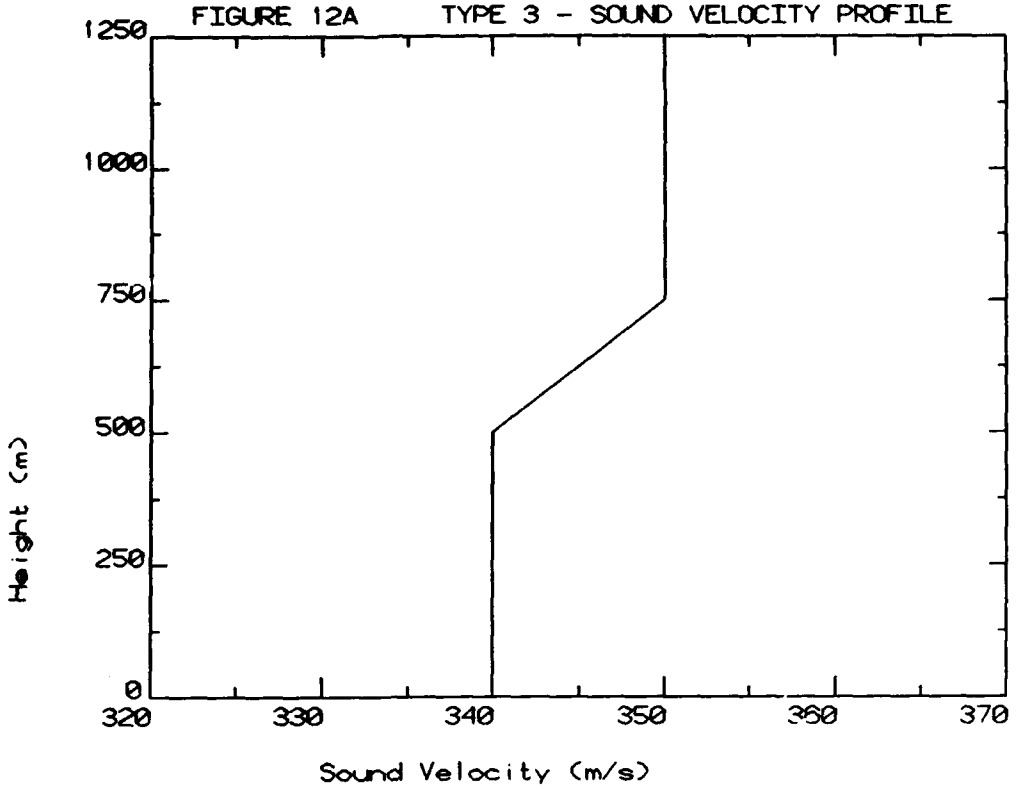

FIGURE 12B TYPE 3 - RANGE vs ELEVATION ANGLE

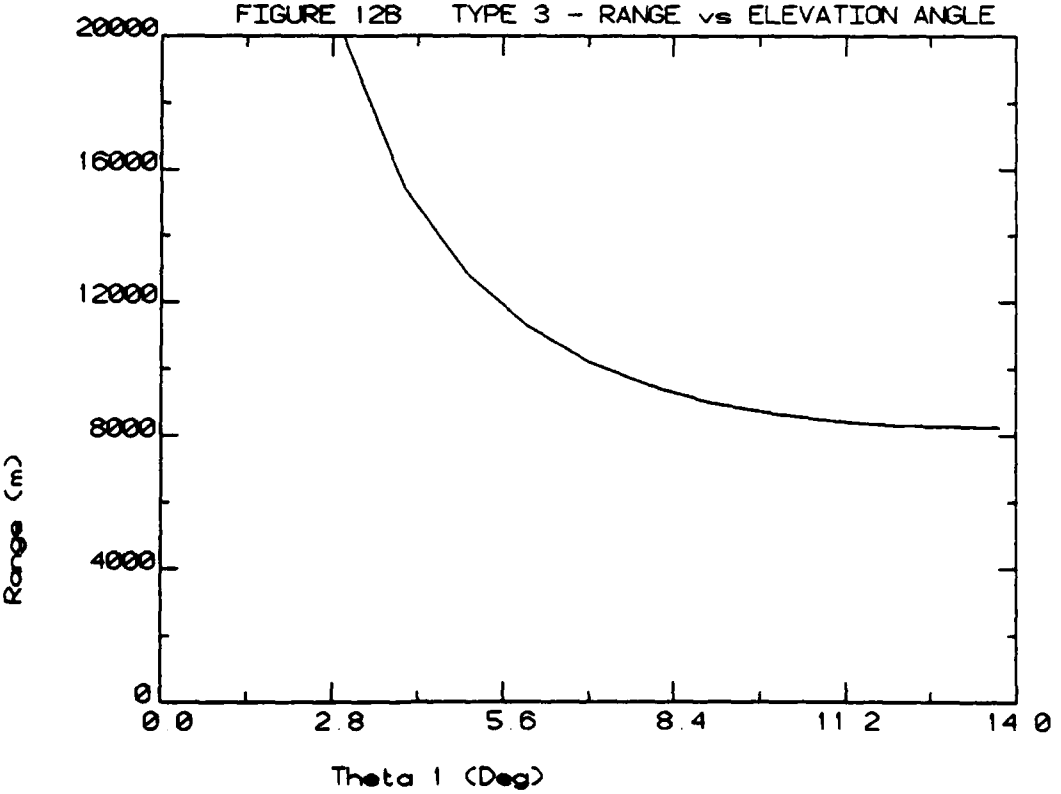

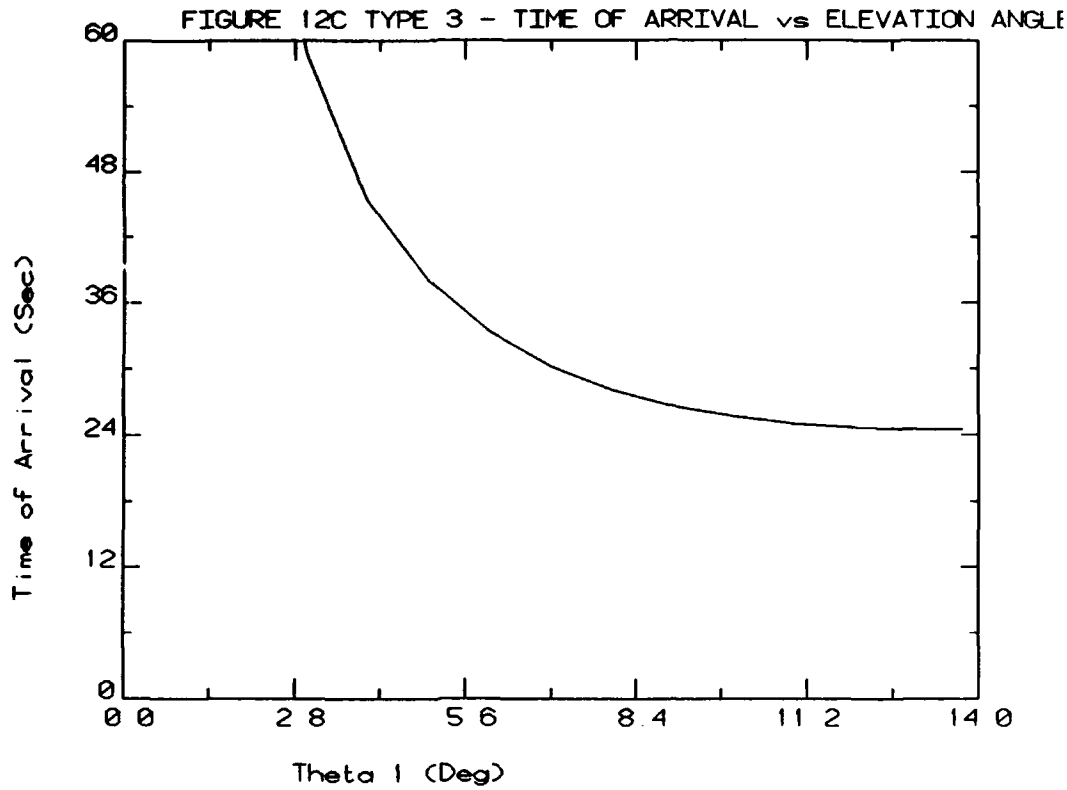
FIGURE 12C TYPE 3 - TIME OF ARRIVAL vs ELEVATION ANGLE
Time of Arrival (Sec)
60
48
36
24
12
0
0 0
2 8
5 6
8 4
11 2
14 0
Theta 1 (Deg)

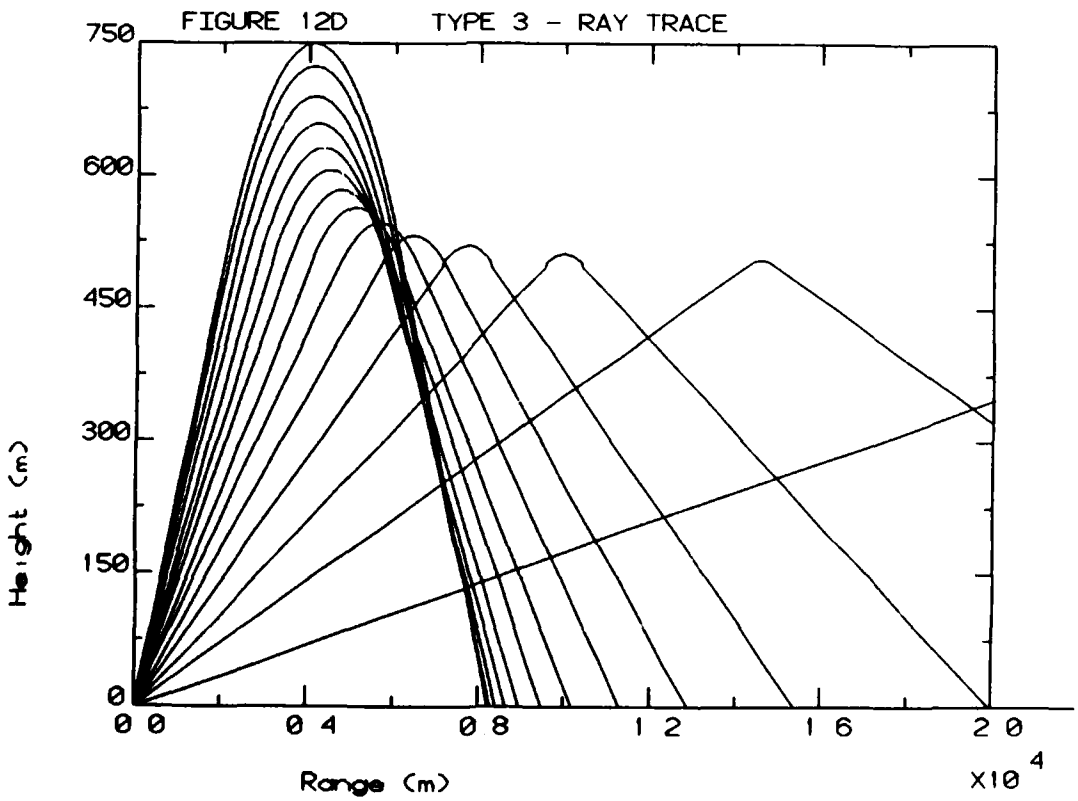
FIGURE 12D TYPE 3 - RAY TRACE
Height (m)
750
600
450
300
150
0
0 0
0 4
0 8
1 2
1 6
2 0
Range (m)
X10 4

FIGURE 13A TYPE 4 - SOUND VELOCITY PROFILE

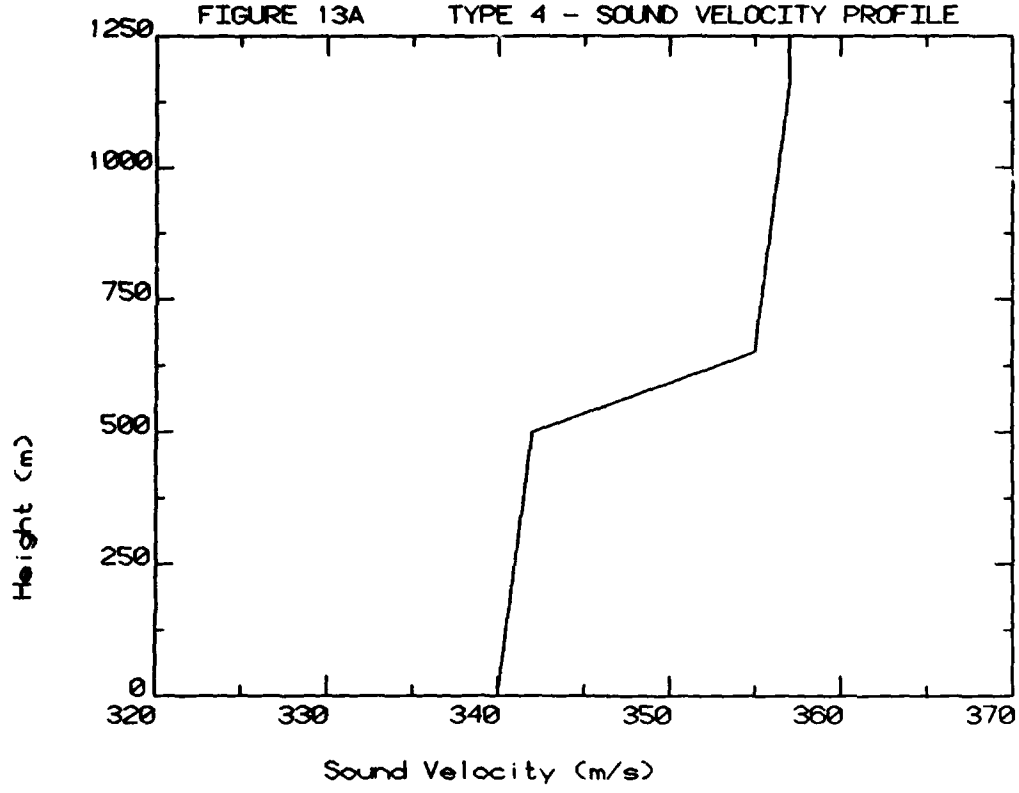

FIGURE 13B TYPE 4 - RANGE vs ELEVATION ANGLE

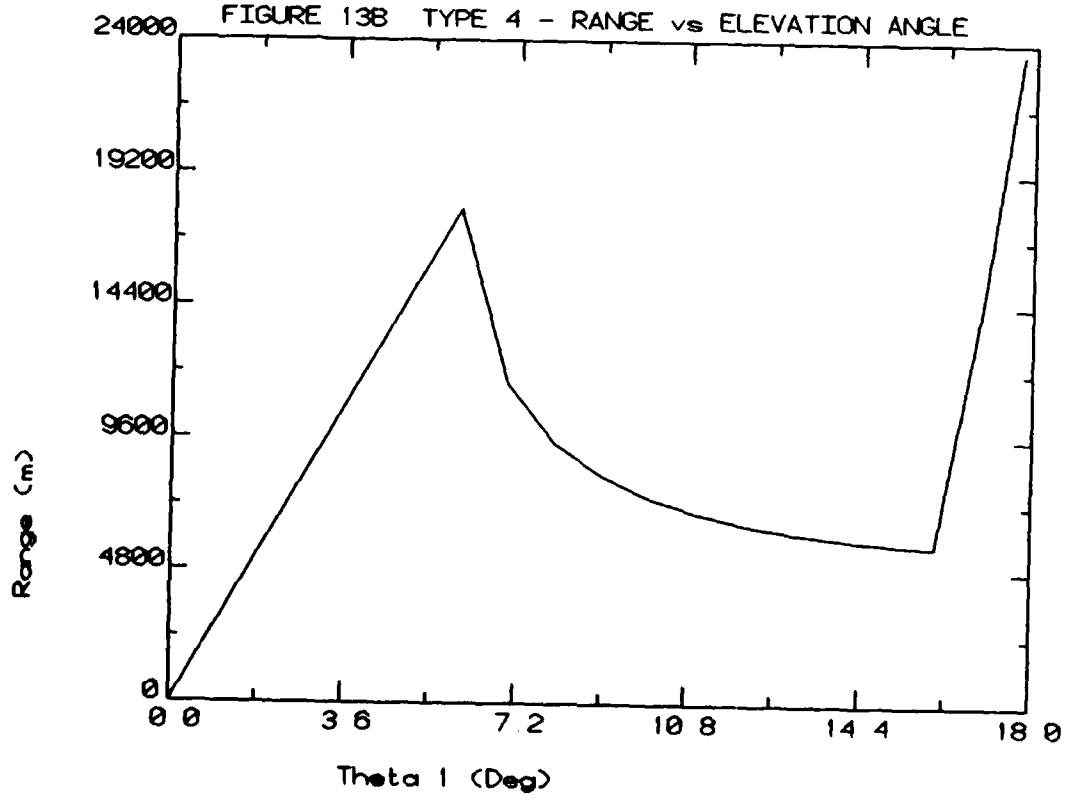

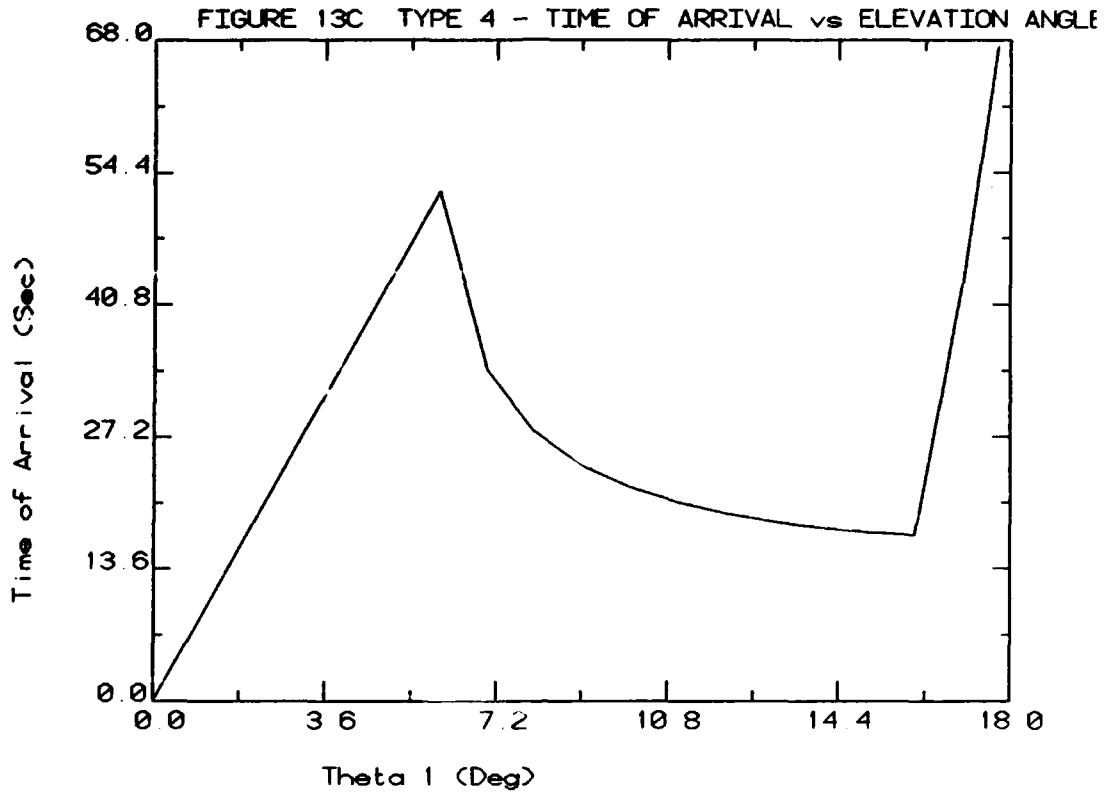
FIGURE 13C TYPE 4 - TIME OF ARRIVAL vs ELEVATION ANGLE
68.0
54.4
40.8
27.2
13.6
0.0
Time of Arrival (Sec)
0.0
3.6
7.2
10.8
14.4
18.0
Theta 1 (Deg)

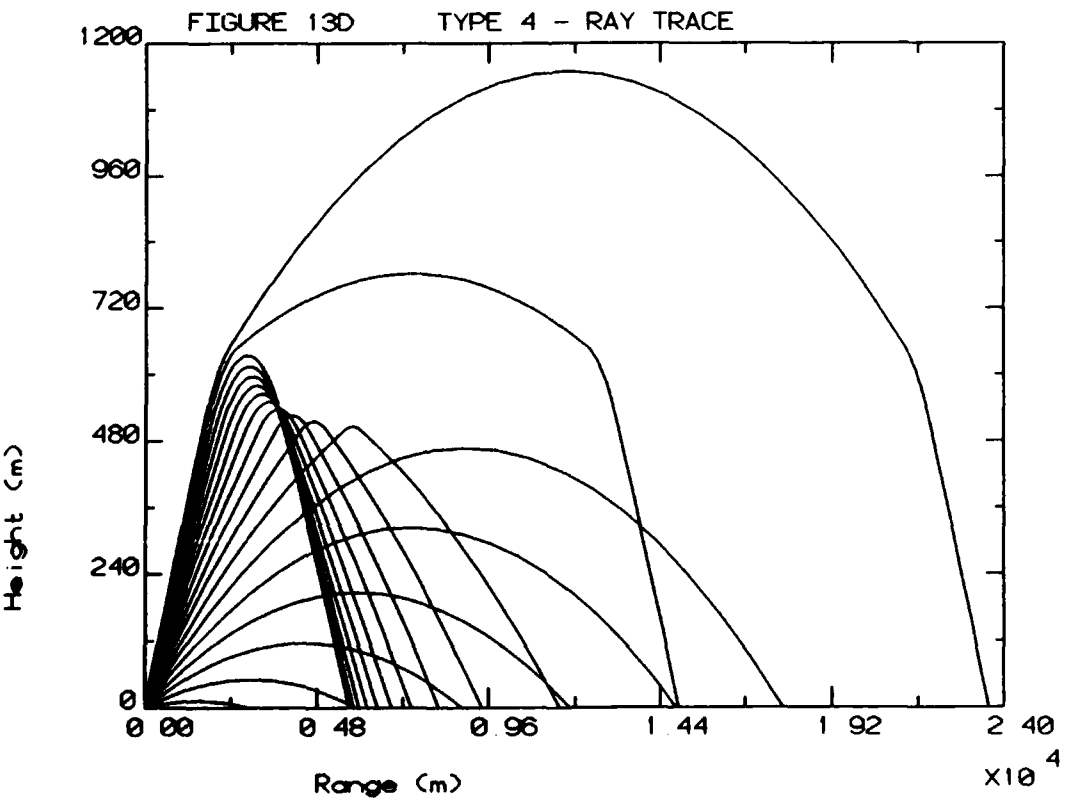
FIGURE 13D TYPE 4 - RAY TRACE
1200
960
720
480
240
0
Height (m)
0.00
0.48
0.96
1.44
1.92
2.40
Range (m)
X10^4

FIGURE 14A TYPE 5 - SOUND VELOCITY PROFILE

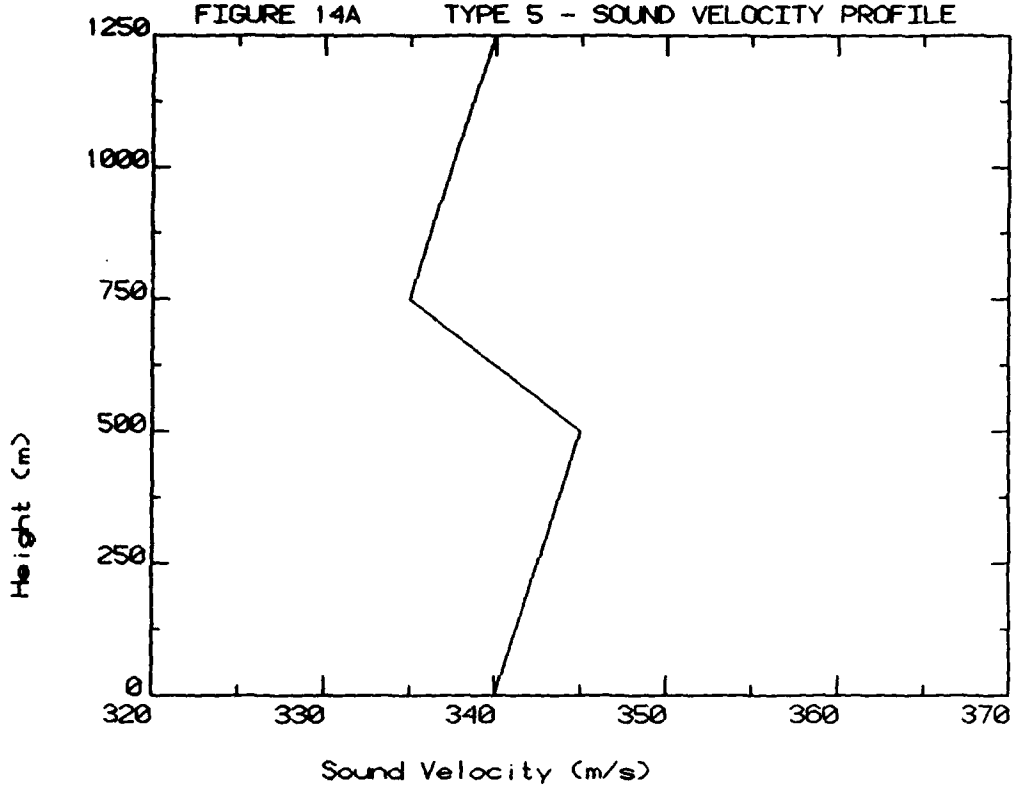

FIGURE 14B TYPE 5 - RANGE vs ELEVATION ANGLE

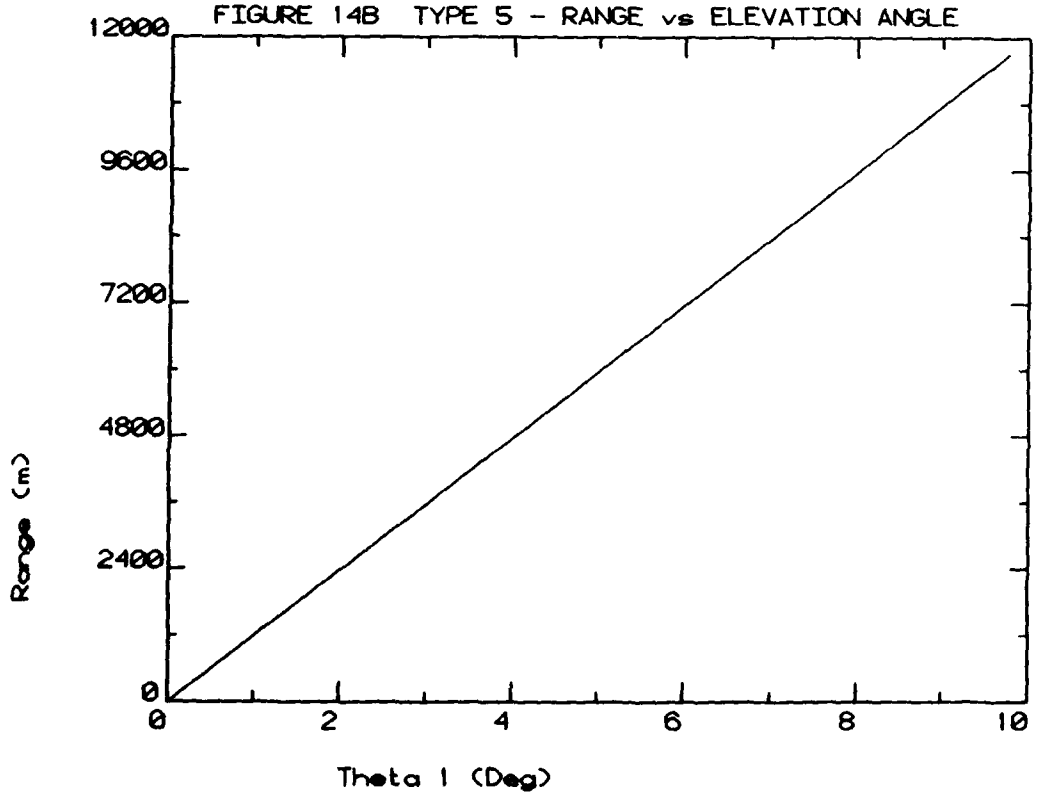

FIGURE 14C TYPE 5 - TIME OF ARRIVAL vs ELEVATION ANGLE

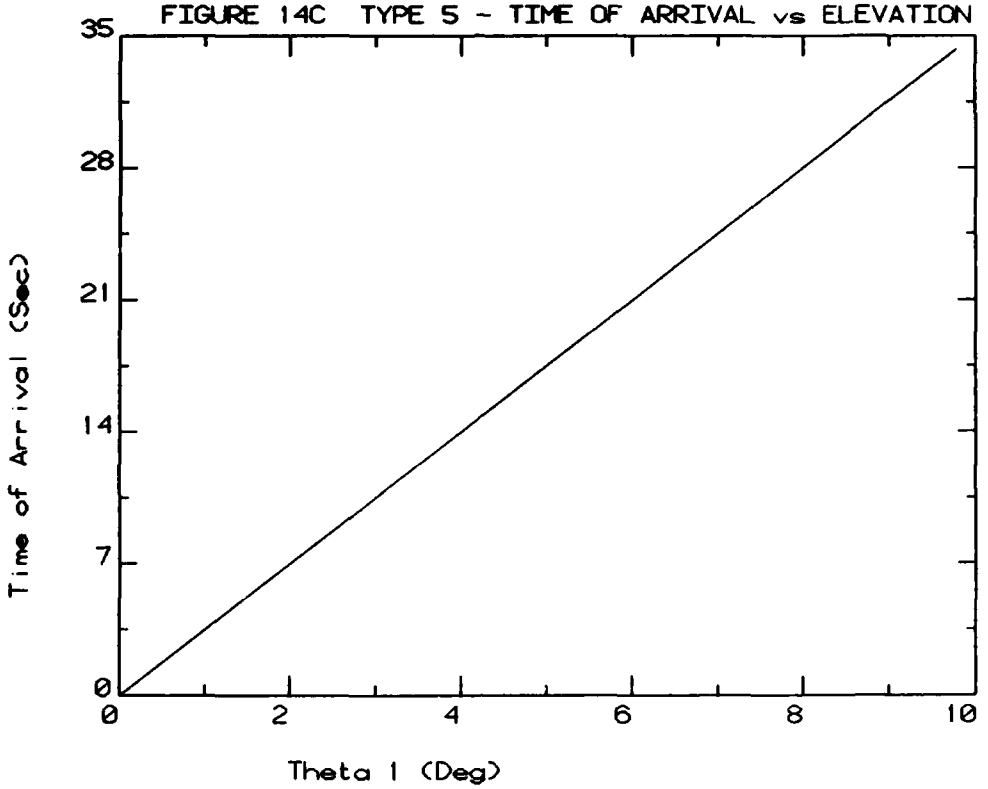

FIGURE 14D TYPE 5 - RAY TRACE

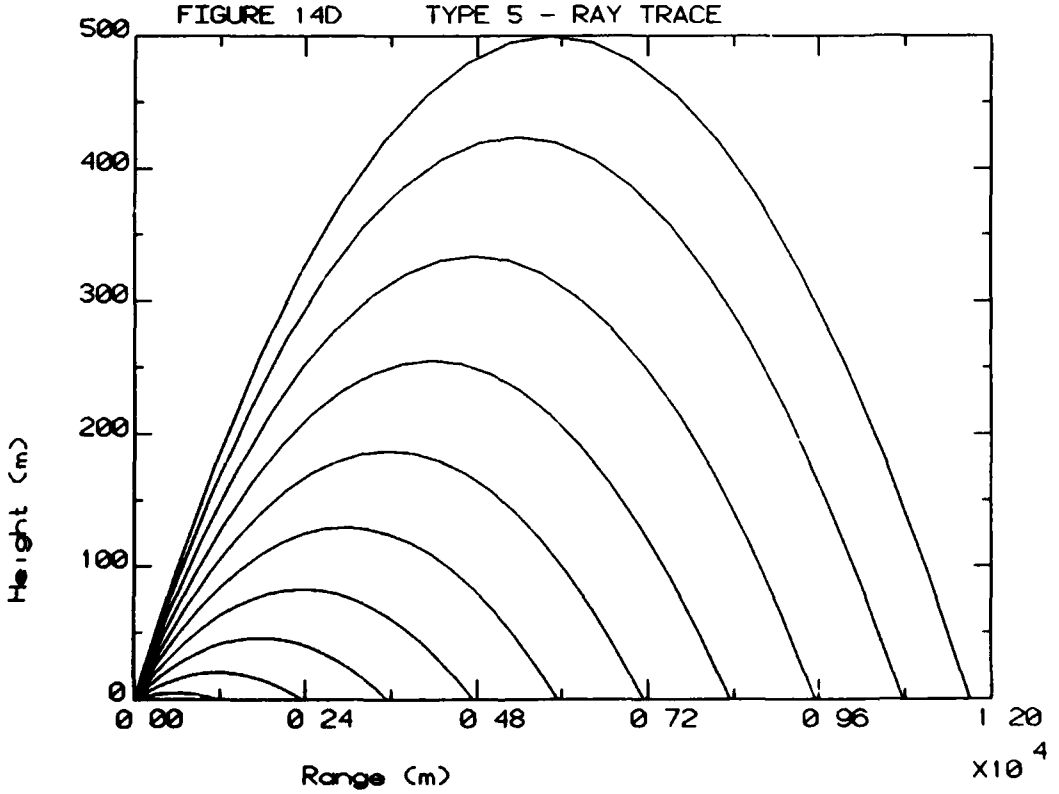

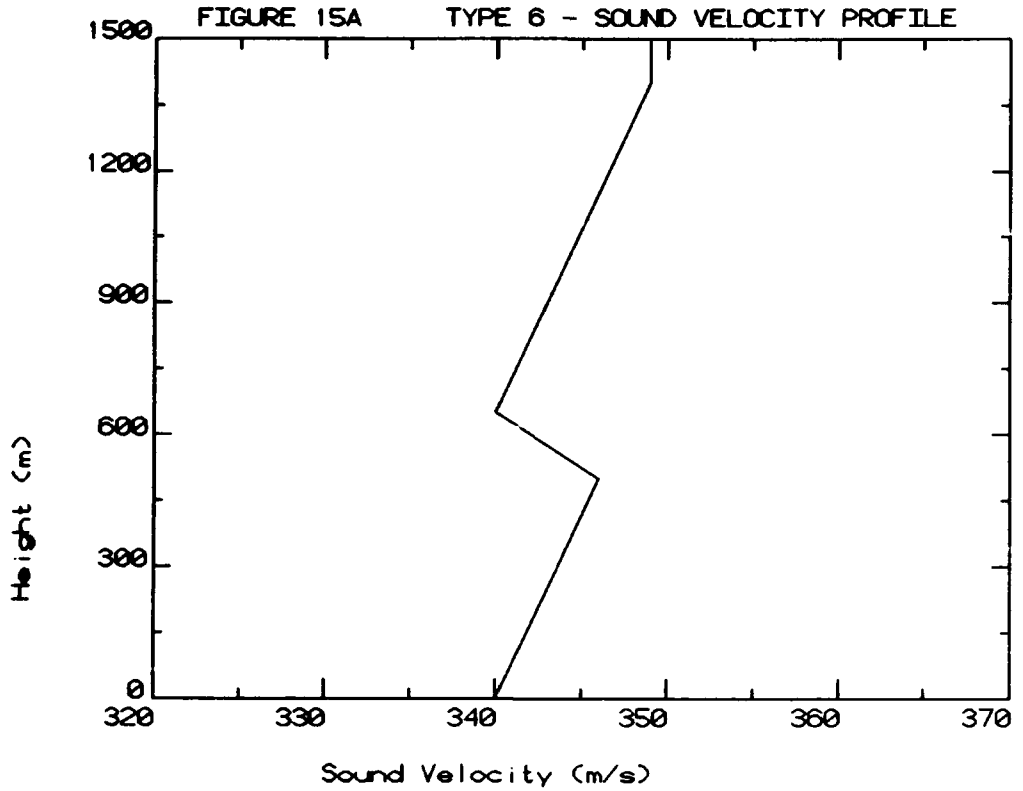
FIGURE 15A TYPE 6 - SOUND VELOCITY PROFILE
1500
1200
900
600
300
0
Height (m)
320
330
340
350
360
370
Sound Velocity (m/s)

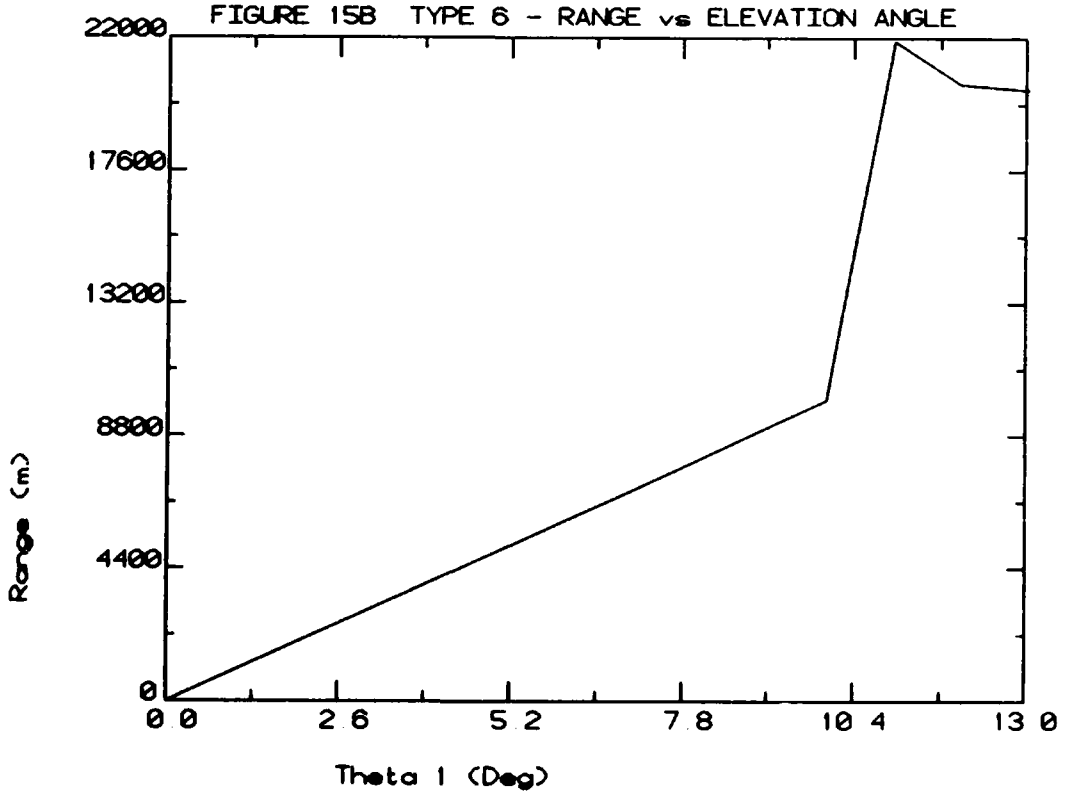
FIGURE 15B TYPE 6 - RANGE vs ELEVATION ANGLE
22000
17600
13200
8800
4400
0
Range (m)
0 0
2 6
5 2
7 8
10 4
13 0
Theta 1 (Deg)

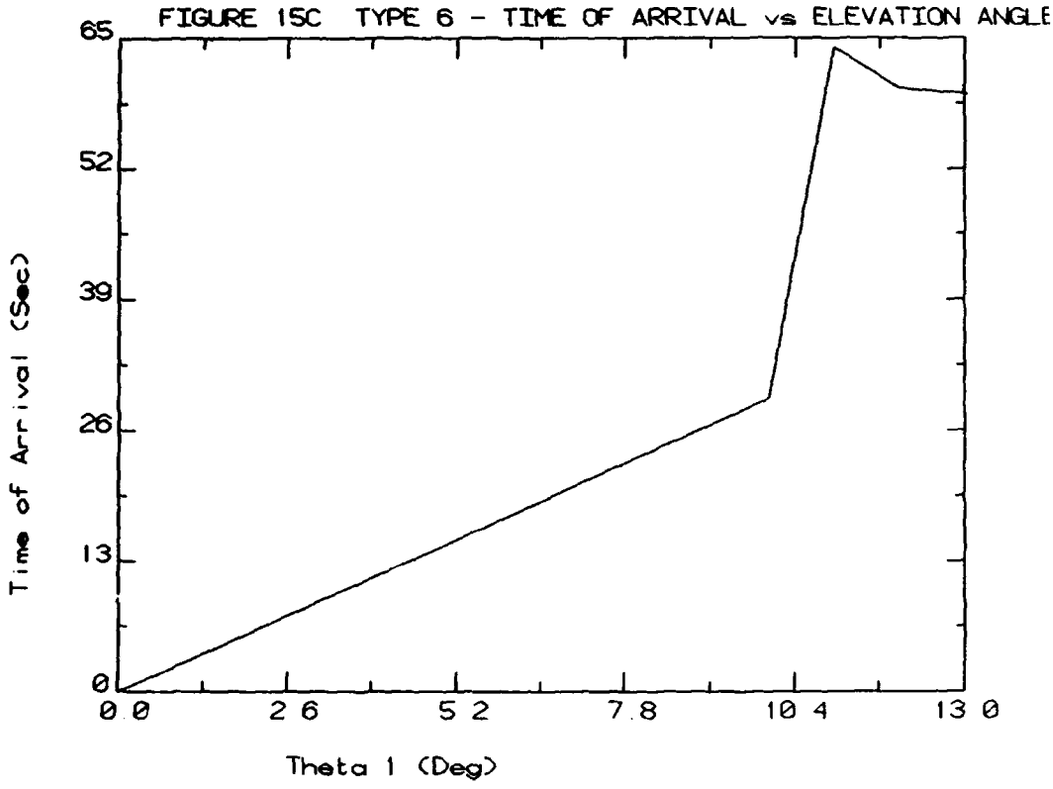
FIGURE 15C TYPE 6 - TIME OF ARRIVAL vs ELEVATION ANGLE
65
52
39
26
13
0
Time of Arrival (Sec)
0 0
2 6
5 2
7 8
10 4
13 0
Theta 1 (Deg)

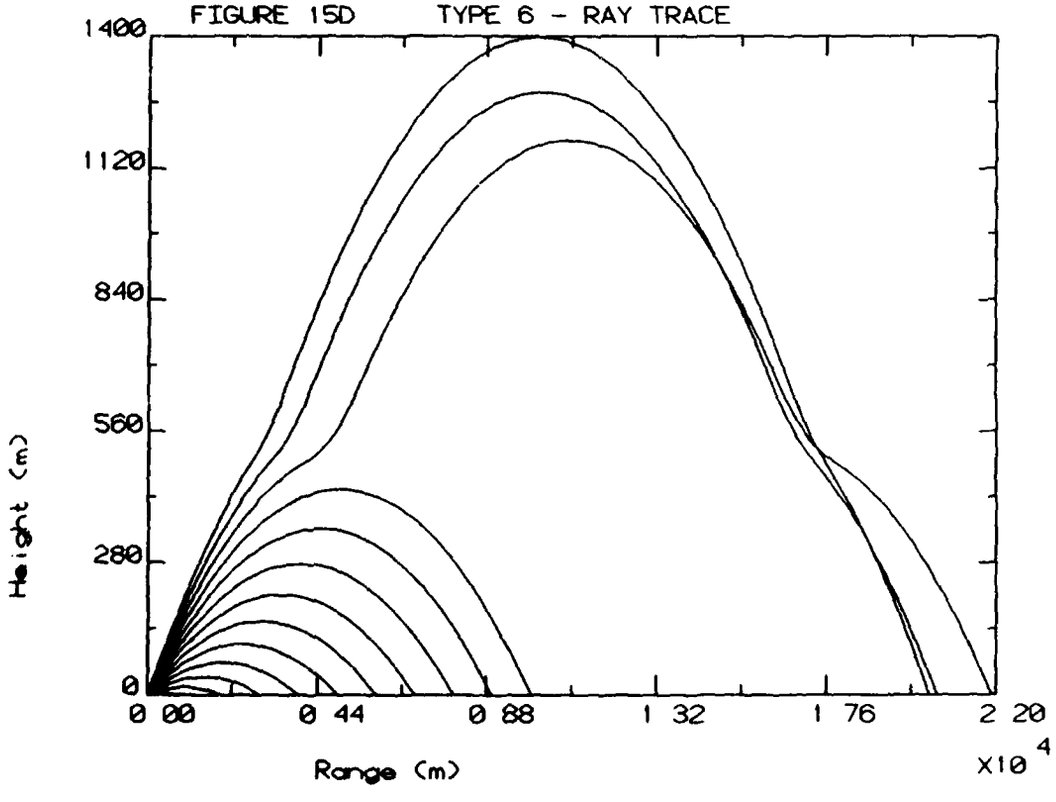
FIGURE 15D TYPE 6 - RAY TRACE
1400
1120
840
560
280
0
Height (m)
0 00
0 44
0 88
1 32
1 76
2 20
Range (m)
X10 4

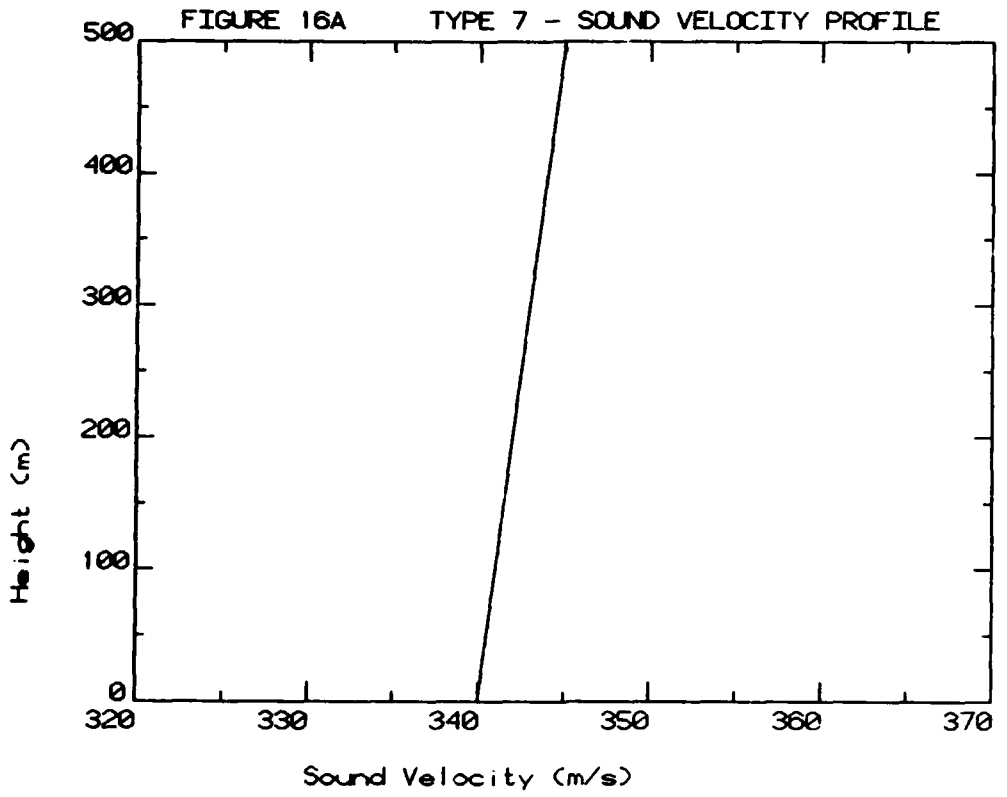
FIGURE 16A TYPE 7 - SOUND VELOCITY PROFILE
500
400
300
200
100
0
320
330
340
350
360
370
Height (m)
Sound Velocity (m/s)

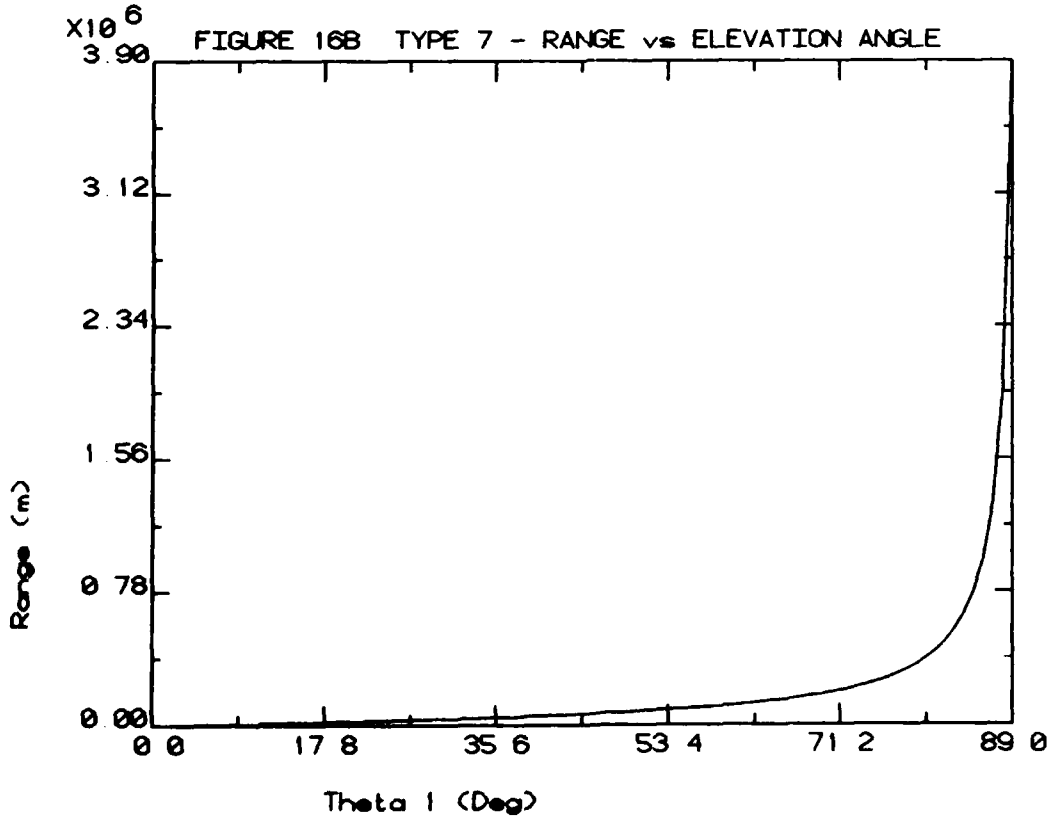
X10 6
FIGURE 16B TYPE 7 - RANGE vs ELEVATION ANGLE
3.90
3.12
2.34
1.56
0.78
0.00
0 0
17 8
35 6
53 4
71 2
89 0
Range (m)
Theta 1 (Deg)

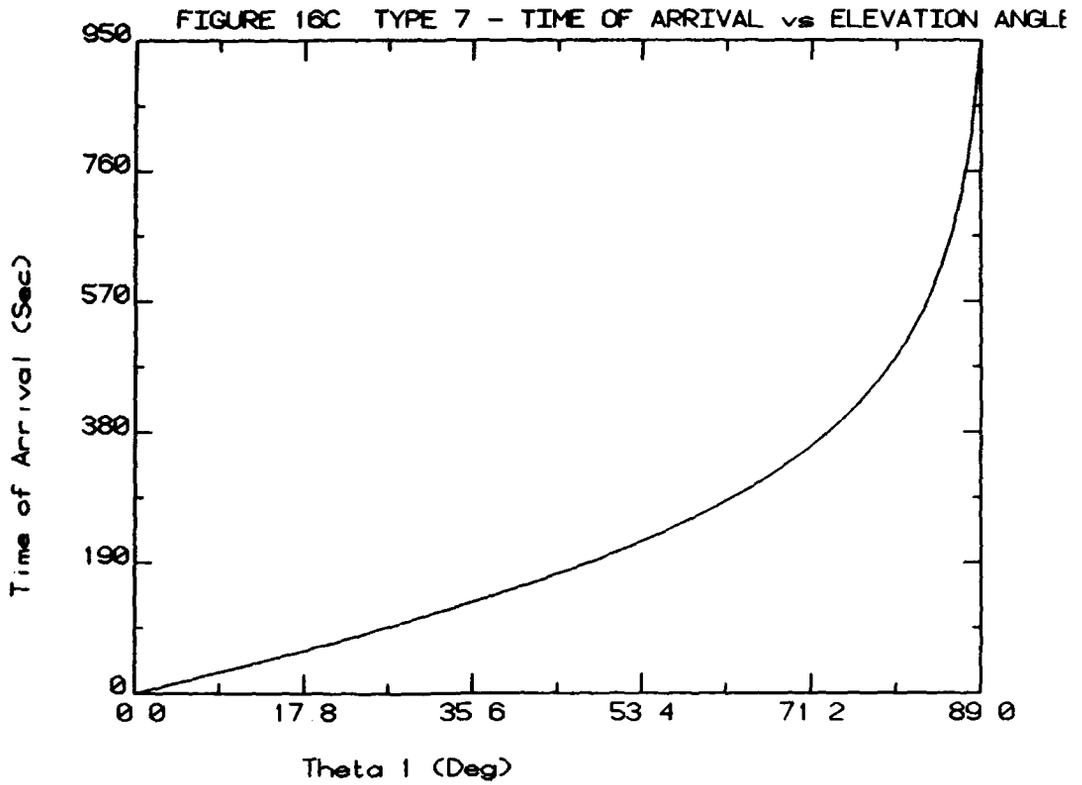
FIGURE 16C TYPE 7 - TIME OF ARRIVAL vs ELEVATION ANGLE
950
760
570
380
190
0
Time of Arrival (Sec)
0 0
17 8
35 6
53 4
71 2
89 0
Theta 1 (Deg)

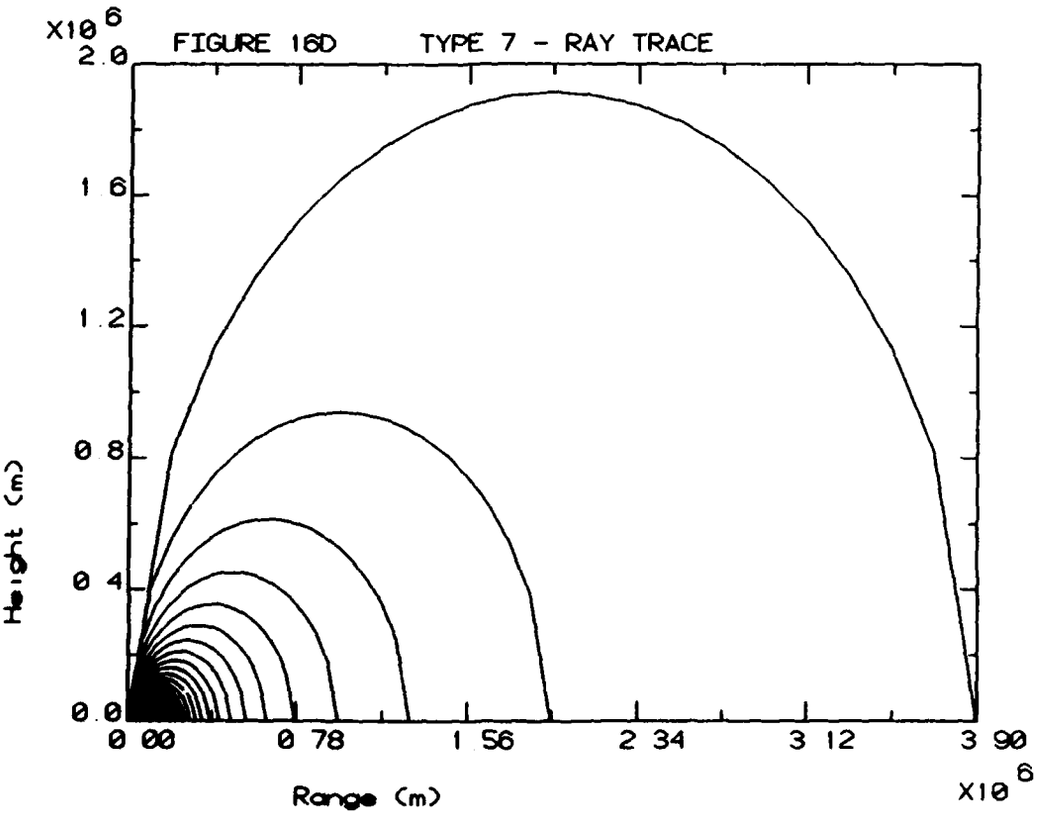
X10 6
2.0
FIGURE 16D TYPE 7 - RAY TRACE
1 6
1 2
0 8
0 4
0.0
Height (m)
0 00
0 78
1 56
2 34
3 12
3 90
Range (m)
X10 6

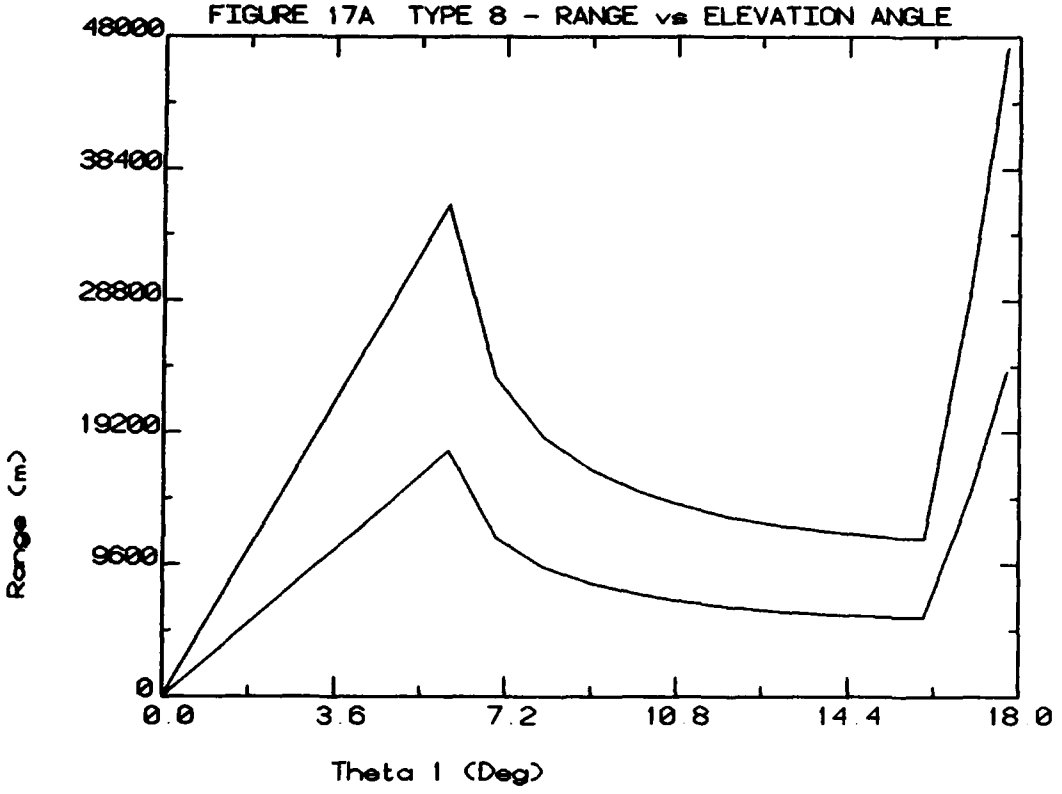

FIGURE 17A TYPE 8 - RANGE vs ELEVATION ANGLE

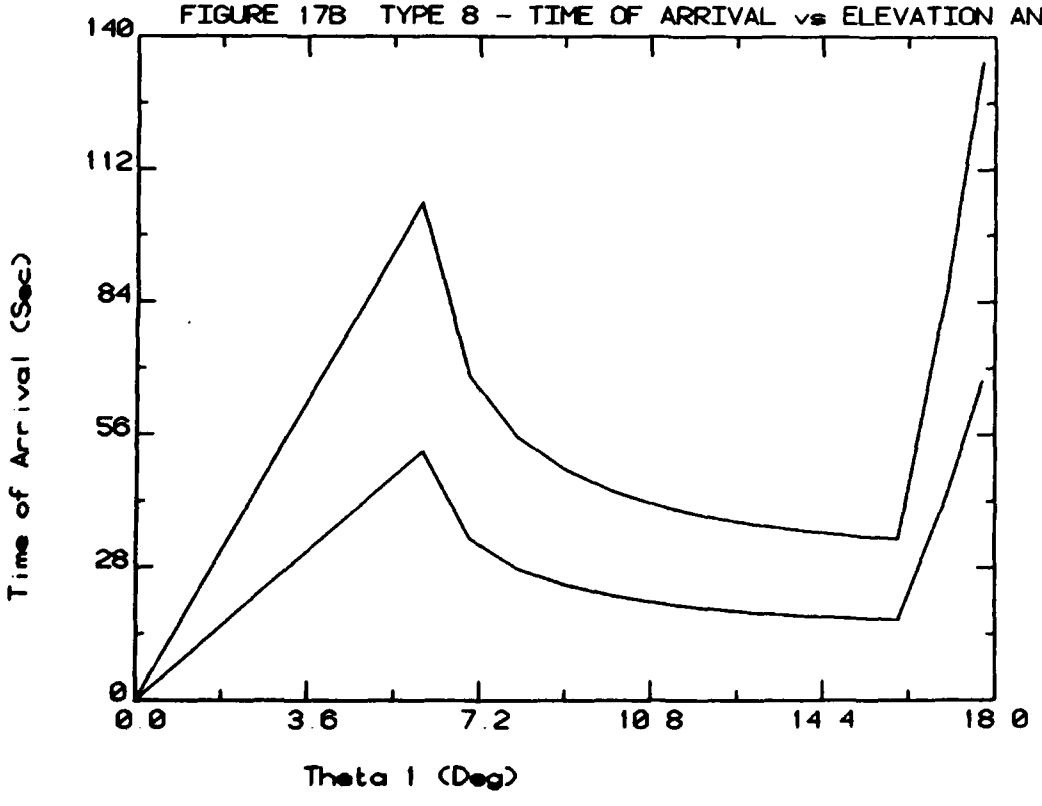

FIGURE 17B TYPE 8 - TIME OF ARRIVAL vs ELEVATION ANGLE

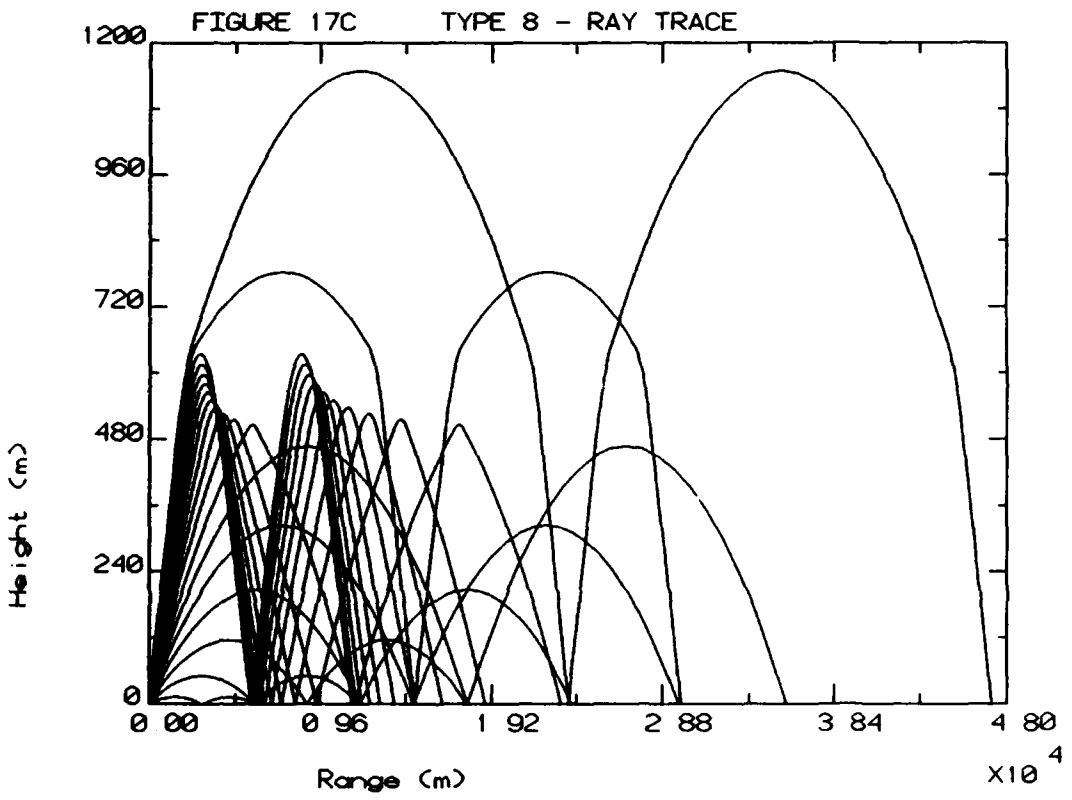
FIGURE 17C TYPE 8 - RAY TRACE
1200
960
720
480
240
0
Height (m)
0 00
0 96
1 92
2 88
3 84
4 80
X10 4
Range (m)

SECURITY CLASSIFICATION OF THIS PAGE **UNCLASSIFIED**

DOCUMENT CONTROL DATA SHEET

REPORT NO.	AR NO.	REPORT SECURITY CLASSIFICATION
MRL-TR-89-10	AR-005-695	Unclassified

TITLE

Focusing of acoustic waves in a non-uniform atmosphere

AUTHOR(S)

G.E. Smith

CORPORATE AUTHOR

Materials Research Laboratory, DSTO
PO Box 50
Ascot Vale Victoria 3032

REPORT DATE	TASK NO.	SPONSOR
May 1989	DST 88/112	DSTO

FILE NO.	REFERENCES	PAGES
G6/4/8-3644	14	60

CLASSIFICATION/LIMITATION REVIEW DATE

CLASSIFICATION/RELEASE AUTHORITY

Chief, Explosives Division MRL

SECONDARY DISTRIBUTION

Approved for public release

ANNOUNCEMENT

Announcement of this report is unlimited

KEYWORDS

Elastic waves
Acoustic velocity
Acoustic radiation
Refraction

SUBJECT GROUPS 0046A

ABSTRACT

The blast scaling principle by charge weights may often produce gross errors in the estimation of overpressures at significant distances from a shot site. The principle ignores weather conditions and assumes a homogeneous atmosphere. Weather conditions may cause variations in the velocity of sound which allows the atmosphere to refract sound waves and act as an acoustic lens. Certain weather conditions such as temperature inversions may allow an acoustic focus many kilometres away from a shot site. Acoustic propagation from a noise producing installation has been mathematically modelled to assist in the prediction of anomalous overpressures by acoustic focusing. MRL has developed a computer model, REFFOCUS, to illustrate foci in a vertically inhomogeneous, non-turbulent, moving atmosphere. The model is produced from sound velocity profiles derived primarily from temperature and wind shear profiles.